

changes according  
to ChiefEditor

changes according to Reviewer1

changes according to Reviewer2

changes according to both Reviewers

# Efficient ensemble generation for uncertain correlated parameters in atmospheric chemical models: a case study for biogenic emissions from EURAD-IM version 5

Annika Vogel<sup>1,2,3</sup> and Hendrik Elbern<sup>1,2</sup>

<sup>1</sup>Institute for Energy and Climate Research - Troposphere (IEK-8), Forschungszentrum Jülich, Germany

<sup>2</sup>Rhenish Institute for Environmental Research at the University of Cologne, Germany

<sup>3</sup>Institute of Geophysics and Meteorology, University of Cologne, Germany

**Correspondence:** A. Vogel, av@eurad.uni-koeln.de

## Abstract.

Atmospheric chemical forecasts highly rely on various model parameters, which are often insufficiently known, as emission rates and deposition velocities. However, a reliable estimation of resulting uncertainties with an ensemble of forecasts is impaired by the high-dimensionality of the system. This study presents a novel approach, which substitutes the problem into

5 a low-dimensional subspace spanned by the leading uncertainties. It is based on the idea that the forecast model acts as a dynamical system inducing multivariate correlations of model uncertainties. This enables an efficient perturbation of high-dimensional model parameters according to their leading coupled uncertainties. The specific algorithm presented in this study is designed for parameters which depend on local environmental conditions and consists of three major steps: (1) an efficient assessment of various sources of model uncertainties spanned by independent sensitivities, (2) an efficient extraction of leading  
10 coupled uncertainties using eigenmode decomposition, and (3) an efficient generation of perturbations for high-dimensional parameter fields by the Karhunen-Loéve expansion. Due to their perceived simulation challenge the method has been applied to biogenic emissions of five trace gases, considering state-dependent sensitivities to local atmospheric and terrestrial conditions.  
Rapidly decreasing eigenvalues state that highly correlated uncertainties of regional biogenic emissions can be represented  
15 by a low number of dominant components. Depending on the required level of detail, leading parameter uncertainties with dimension of  $\mathcal{O}(10^6)$  can be represented by a low number of about 10 ensemble members. This demonstrates the suitability of the algorithm for efficient ensemble generation for high-dimensional atmospheric chemical parameters.

## 1 Introduction

Due to highly nonlinear properties of the atmosphere including its chemistry, forecast uncertainties vary significantly in space and time and among variables. During the last decades, increasing efforts have been put into estimating forecast uncertainties  
20 induced by different error sources. In this context, the method for generating an ensemble of forecasts is crucial as it determines the forecast probability distribution. While the represented details of the probability distribution increase with the number of realizations, the ensemble size of high-dimensional atmospheric systems is limited by computational resources (Leutbecher,

2019). Thus, the major challenge is the generation of ensembles which sufficiently sample the forecast uncertainty within manageable computational efforts. This renders ensemble forecasting one of the most challenging research areas in atmospheric  
25 modeling (e.g. Bauer et al., 2015; Buizza, 2019).

In numerical weather prediction (NWP), different ensemble methods have been developed in order to account for uncertainties of initial conditions and the forecast model formulation. First studies were motivated by the fact that initial conditions induce dominant uncertainties to NWP systems. Bred vectors (BV, Toth and Kalnay, 1993) or Singular vectors (SV, Buizza et al., 1993) are used to efficiently generate initial perturbations along the directions of the fastest growing errors in a linearized  
30 or nonlinear forecast model, respectively. Another approach estimates uncertainties of initial conditions by applying random perturbations to observations (PO, Houtekamer et al., 1996) which are assimilated in the modeling system.

As errors in initial conditions cannot entirely explain forecast errors, two methods related to uncertainties within the NWP model have been developed. Firstly, the stochastic kinetic energy backscatter scheme (SKEBS, Shutts, 2005) accounts for uncertainties in the amount of energy which is backscattered from subgrid to resolved scales. The second group of methods  
35 focuses on uncertainties in model parameterizations, which rely on simplified assumptions about non-resolved processes. In the stochastic parameter perturbation scheme (SPP, Houtekamer et al., 1996), selected parameters within individual parameterizations are multiplied with random numbers. In contrast, the stochastically perturbed parameterization tendencies scheme (SPPT, Buizza et al., 1999) considers uncertainties in the formulation of the parameterization schemes itself. Instead of perturbing individual parameters, total tendencies of state variables from all parameterizations are multiplied with appropriately  
40 scaled random numbers. Although perturbations are generated in a spatially and temporally correlated way, both, correlation scales and standard deviations of the random numbers are predefined as fixed values (e.g., Leutbecher et al., 2017; Lock et al., 2019).

While different methods for ensemble generation are successfully applied to NWP, less approaches are available for chemistry transport modeling. As chemistry transport models (CTMs) include a large number of trace gases and aerosol compounds,  
45 the dimension of the system is even higher than in NWP (Zhang et al., 2012a). Among other implications, this high-dimensionality amplifies the amount of uncertainties which differ significantly between individual chemical compounds (Emili et al., 2016). In the context of atmospheric data assimilation, reduced rank square-root Kalman filter approaches (Cohn and Todling, 1996; Verlaan and Heemink, 1996) have been successfully applied to reduce the high-dimensional covariance matrix to a small number leading eigenmodes (e.g., Auger and Tangborn, 2004; Hanea et al., 2004; Hanea and Velders, 2007). Additionally, the temporal evolution of atmospheric chemical forecast errors differs from typical error growth characteristics in NWP. This inhibits a straightforward application of existing ensemble generation approaches from NWP to CTMs.

Besides using multi-model ensembles for estimation of forecast uncertainties (e.g., McKeen et al., 2007; Xian et al., 2019), there are only few attempts for ensemble generation within a single CTM. As CTMs are driven by meteorological forecasts,  
55 uncertainties in NWP are transferred to the chemical simulations. A comparably simple approach, which was used by Vautard et al. (2001) for the first time, employs an existing meteorological ensemble to drive the atmospheric chemical forecasts. However, estimations of chemical uncertainties solely driven by NWP ensembles do not necessarily represent related uncertainties

in CTMs. For example, Vogel and Elbern (2021a) note that a global meteorological ensemble was not able to induce significant ensemble spread in surface-near forecasts of biogenic trace gases.

Multiple studies indicate that uncertainties of CTMs are mainly induced by uncertain model parameters – controlling emissions, chemical transformation and deposition processes – rather than initial conditions or meteorological forecasts (e.g., Elbern et al., 2007; Bocquet et al., 2015). Consequently, former attempts aim to account for uncertainties in model parameters or other chemical input fields (for an overview see Zhang et al., 2012b, and references therein). However, perturbing parameter fields appears to suffer from the high-dimensionality of the system as independent perturbations of model parameters at each location and time remains impractical. Early studies like the one performed by Hanna et al. (1998) assume predefined uncertainties where perturbations are applied uniformly in space and time, ignoring any cross-correlations between parameters. This uniform perturbation of model parameters with a fixed standard deviation is still applied to emissions in the context of ensemble data assimilation (e.g., Schutgens et al., 2010; Candiani et al., 2013).

However, constant perturbation of the whole parameter field does not allow for any spatial variation within the domain. More recently, limited spatial correlations are considered in uncertainty estimation by uniform perturbations within arbitrary subregions (Boynard et al., 2011; Emili et al., 2016) or isotropic decrease with fixed correlation length scales (Gaubert et al., 2014). Although recent approaches allow a local treatment of correlations, they are not able to represent the spatio-temporal properties of the dynamical system. Already Hanna et al. (1998) propose that introducing state-dependent uncertainties as well as cross-correlations between parameters would provide a more realistic representation.

The Karhunen-Loéve (KL) expansion provides an opportunity to account for such complex correlated uncertainties based on eigenmode decomposition. While this approach is well established in engineering, it has rarely been applied in geophysical sciences. Siripatana et al. (2018) used the KL expansion for dimension reduction in an idealized oceanographic ensemble data assimilation setup. The eigenmode analysis required for the KL expansion is equivalent to a principal component analysis (PCA) by singular vector decomposition (SVD). The discrete PCA has been used as diagnosis tool in atmospheric sciences and is most established in climatology (e.g., Hannachi et al., 2007; Galin, 2007; Liu et al., 2014; Guilloteau et al., 2021). Goris and Elbern (2015) performed singular vector decomposition to determine optimal placement of trace gas observation sites. To the knowledge of the authors, the KL expansion has not been used for ensemble generation in atmospheric chemical models.

In order to address this issue, this study introduces a novel approach for optimized state-dependent parameter perturbation in atmospheric chemical models. The approach is based on the idea that the dynamical system induces multivariate correlations of model states and uncertainties. In particular, the algorithm aims to provide (1) an efficient assessment of various sources of uncertainties, (2) an efficient extraction of leading coupled uncertainties, and (3) an efficient generation of perturbations for high-dimensional parameter fields. Section 2 provides the concept of sensitivity estimation on which the ensemble generation approach is based. The specific algorithm presented in Sect. 3 is designed for model parameters, which depend on model arguments like model inputs and configurations. Representative performance results are presented in Sect. 4 for biogenic emissions representing a highly uncertain, yet correlated set of parameters. A discussion on benefits and limitations of the presented approach is given in Sect. 5. Finally, Sect. 6 provides a summary and conclusions of this study.

## 2 Concept of Sensitivity Estimation

This section introduces the conceptual basis for the description of the ensemble generation algorithm in Sect. 3. The algorithm relies on several definitions which are introduced in Sect. 2.1. Given these definitions, the concept of sensitivities consists of two parts: the general formulation of sensitivities in Sect. 2.2, and the special formulation of independent sensitivities 95 in Sect. 2.3. Each of these parts provides the basis for combined or independent covariance construction in the ensemble generation algorithm, respectively.

### 2.1 Definitions

The concept of sensitivity estimation requires the definition of several terms. This section introduces these terms on a general level and provides examples for the application to CTMs. All important terms used in the concept of sensitivity estimation and 100 the algorithm are summarized in Tab. 1, including specific examples for the application to biogenic emissions.

Generally, the term *model parameter* refers to any parameter in the prognostic equations of the model which may affect the models forecast. A prominent example of highly uncertain model parameters in CTMs are trace gas emissions. Considering multiple model parameters, like the emission rates of different trace gases, the *dimension N* of the problem is the total number of all considered parameters at all grid-boxes. The total set of all parameter values at all grid-boxes at time  $t$  is denoted by 105 vector  $Q(t) \in \mathcal{R}^N$ . In the case of trace gas emissions,  $Q(t)$  includes the simulated emission rates of all considered gases at all grid-boxes. Thus, the  $n$ -th entry  $Q^{s_n}(t)$  of the parameter vector is the simulated value of model parameter  $p_n$  at grid-box  $(x_n, y_n, z_n)$ . The index  $s_n = (p_n, x_n, y_n, z_n)$  specifies the model parameter and grid-box and is therefore denoted as *position*. Hence, the positions of all parameters at all grid-boxes is given by the *index set*  $S := \{s_1, s_2, \dots, s_N\}$ .

The concept of sensitivities uses a set of  $J$  parameter vectors  $Q_j(t)$  from differently configured model simulations  $j \in [1, J]$ . 110 In this approach, different model simulations are achieved by using different implementations  $r_i$  of a set of model arguments  $i \in [1, I]$ . The term *model argument* comprises a heterogeneous set of available arguments for the specific configuration of the model. In this regard, model arguments in CTMs may be as diverse as initial and boundary conditions, any external input fields and the formulation of parameterizations in the model. The specific *implementation*  $r_i$  of a model argument  $i$  is realized by selecting one available option of the argument in the model. For example, input fields of land surface properties may be 115 one model argument with two implementations: land surface information from source A and from source B. In the concept of sensitivity estimation, each model argument  $i \in [1, I]$  is interpreted as arbitrary parameter with  $R_i$  different implementations  $r_i \in [1, R_i]$ . Thus, each *setup index*  $j \in [1, J]$  represents a complete *model setup*  $\{r_1, r_2, \dots, r_I\}$  as specific combination of implementations  $r_i$  of each model argument  $i \in [1, I]$ . Then  $Q_j^s(t)$  is the parameter value of position  $s \in S$  simulated with model 120 setup  $j \in [1, J]$  at discrete time  $t \in [t_1, t_T]$ . Note that the complete set of  $\{Q_j^s(t)\}_{j \in [1, J]}$  considers all possible combinations of implementations of all model arguments.

**Table 1.** Notations used in the concept of sensitivity estimation and the formulation of the algorithm including examples.

Term	Expression	Description	Examples of the application to biogenic emissions
<b>(Model) Parameter</b>	$Q_j^s(t)$	Parameter value from model setup $j$ at time $t$ and position $s$ .	Biogenic emission rate from model setup $j$ at time $t$ and position $s$
	$q_i^s(r_i, t)$	Parameter value from setup where only the $i$ -th argument differs from reference setup $r_i \neq r_{i*}$ . $\{q_i^s(r_i, t)\} \subset \{Q_j^s(t)\}$	
<b>Dimension</b>	$N$	Dimension of the problem (total number of elements in the set of considered model parameters).	5 parameters at 6.572 land surface grid-boxes $\Rightarrow N = 32.860$
<b>Index Set</b>	$S = \{s_1, s_2, \dots, s_N\}$	Set of indices representing the positions of all perturbed model parameters $p$ at all grid boxes $(x, y, z)$ .	$S = \{(p_1, x_1, y_1, z_1), (p_2, x_1, y_1, z_1), (p_3, x_1, y_1, z_1), \dots\}$
— Position	$s_n \in S$	$n$ -th element in the index set representing the position of parameter $p_n$ at grid box $(x_n, y_n, z_n)$ .	e.g. $s_1 = (p_1, x_1, y_1, z_1)$ / $s_2 = (p_2, x_1, y_1, z_1)$ / $s_3 = (p_3, x_1, y_1, z_1)$ / ...
<b>(Model) Argument</b>	$i \in [1, I]$	Arguments in the model configuration including the specification of initial conditions, input fields and model parameterizations.	$I = 6$ : land use information / global meteorology / land surface model / boundary layer- / microphysics- / radiation parameterization
<b>Implementation</b>	$r_i \in [1, R_i]$	Available options of each model argument $i$ .	$R_i = 2 \forall i$ : e.g. $r_1 = 1 \rightarrow$ USGS land use / $r_1 = 2 \rightarrow$ MODIS land use, $r_2 = 1 \rightarrow$ ECMWF global meteo / $r_2 = 2 \rightarrow$ GFS global meteo, ...
— Reference Implementation	$r_{i*}$	Selected reference implementation of each model argument.	$r_{i*} = 1 \forall i$ (USGS land use, ECMWF global meteo, ...)
<b>(Model) Setup</b>	$\{r_1, r_2, \dots, r_I\}$	Specific set of implementations $r_i$ of all model arguments $i$ .	— e.g. $\{1, 1, 1, 1, 1, 1\}$ / $\{1, 1, 1, 1, 1, 2\}$ / $\{1, 1, 1, 1, 2, 1\} / \dots / \{2, 2, 2, 2, 2, 2\}$
— Setup Index	$j \in [1, J]$	Index indicating one specific model setup.	— e.g. $j = 1 \rightarrow \{1, 1, 1, 1, 1, 1\}$ / $j = 2 \rightarrow \{1, 1, 1, 1, 1, 2\} / \dots / j = J \rightarrow \{2, 2, 2, 2, 2, 2\}$
— Reference Setup	$j_* \rightarrow \{r_{1*}, r_{2*}, \dots, r_{I*}\}$	Index of reference setup representing the set of reference implementations $r_{i*}$ of all model arguments $i$ .	$j_* = 1 \rightarrow \{1, 1, 1, 1, 1, 1\}$
<b>Sensitivity Factor</b>	$F_j^s$	Temporally averaged amplification factor of model setup $j$ at position $s$ w.r.t. the reference setup $j_*$ (see Eq. (1)).	
— Independent Factor	$f_i^s(r_i)$	Sensitivity factor w.r.t. single model argument $i$ with implementation $r_i \neq r_{i*}$ differing from the reference (assumed to be independent of other arguments).	
<b>Sensitivity</b>	$X_j^s$	Sensitivity to model setup $j$ at position $s$ (see Eq. (2)).	
— Independent Sensitivity	$x_i^s(r_i)$	Sensitivity w.r.t. single model argument $i$ with $r_i \neq r_{i*}$ (assumed to be independent of other arguments).	
<b>Perturbation</b>	$Y_{\omega_p}^s$	Perturbation as $p$ -th random realization of the KL expansion at position $s$ (see Eq. (15)).	
<b>Perturbation Factor</b>	$F_{\omega_p}^s$	Perturbation factor to be applied to the model parameter at position $s$ of the $p$ -th member in the ensemble forecast.	Emission factor of the $p$ -th member multiplied to biogenic emissions at position $s$ .

## 2.2 Formulation of Sensitivities

The formulation of state-dependent sensitivities is based on Elbern et al. (2007) who demonstrated the suitability of amplification factors in the context of 4D-variational optimization of emissions. Let  $j_*$  be a *reference model setup* (here  $j_* := 1$ ) representing the selected *reference implementation*  $r_{i*} = 1$  of each model argument  $i \in [1, I]$ . Then, the model parameter 125  $Q_j^s(t)$  of model setup  $j$  at time  $t$  and position  $s$  is divided by its corresponding value from the reference configuration  $Q_{j_*}^s(t)$ . The *sensitivity factor*  $F_j^s$  is defined as temporal average of those over the time interval  $[t_1, t_T]$ :

$$F_j^s := \frac{1}{T} \sum_{t=t_1}^{t_T} \frac{Q_j^s(t)}{Q_{j_*}^s(t)} \quad \forall j \in [1, J], s \in S. \quad (1)$$

Depending on the type of model parameter, the sensitivity factors may not be Gaussian distributed. This is especially true for parameters which are positive by definition, like emissions of trace gases. Analogous to emission factors in Elbern et al. (2007), 130 sensitivity factors of emissions are assumed to be lognormally distributed. In this case, the sensitivity factors are substituted to normally distributed *sensitivities*  $X_j^s$  in order to simplify their further treatment:

$$X_j^s := \ln(F_j^s) \quad \forall j \in [1, J], s \in S. \quad (2)$$

Since the definition of sensitivities refers to all possible combinations of implementations of all model arguments, the set of 135  $\{X_j^s\}_{j \in [1, J]}$  is also denoted as set of *combined sensitivities*. Given  $R_i$  implementations  $r_i \in [1, R_i]$  of each model argument  $i \in [1, I]$ , the total number of combined sensitivities  $X_j^s$  with  $j \in [1, J]$  is

$$J_{\text{combi}} := J = \prod_{i=1}^I R_i. \quad (3)$$

For atmospheric model parameters, each sensitivity  $X_j^s$  requires its own forecast simulation. Thus, the calculation of all combined sensitivities becomes computationally demanding even for a low number of implementations of a few model arguments. Figure 1 shows the exponential increase of the number of combined sensitivities as function of the number of implementations and arguments from Eq. (3). For example, considering six model arguments ( $I = 6$ ) with two implementations each 140 ( $R_i = 2, \forall i \in [1, I]$ ), requires  $J_{\text{combi}} = J = 2^6 = 64$  model executions prior to the ensemble generation.

## 2.3 Formulation of Independent Sensitivities

As this study aims for an computationally efficient algorithm focusing on leading uncertainties, the computational efforts required for the estimation of sensitivities are critical. Thus, a new method for efficient sensitivity estimation is introduced, 145 which reduces the number of required model executions prior to ensemble generation significantly. Instead of using all possible combinations of model arguments, the method uses only sensitivities with respect to single model arguments. By assuming tangent linearity of sensitivities in the limits of imposed perturbations, these sensitivities are extrapolated to approximate the full set of combined sensitivities.

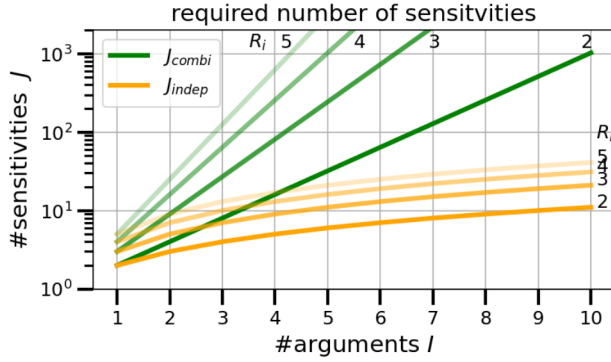


**Figure 1.** Number of required sensitivities as function of the number of arguments  $I$ . Shown are the required numbers of combined ( $J_{\text{combi}}$ , Eq. (3), green) and independent ( $J_{\text{indep}}$ , Eq. (8), orange) sensitivities for different numbers of implementations  $R_i = 2, 3, 4, 5 \quad \forall i \in [1, I]$ .

The assumption of tangent linearity equals mutual independence of the model arguments and thus every combined sensitivity factor  $F_j^s$  with arguments  $\{r_1, r_2, \dots, r_I\}$  can be decomposed into a set of *independent sensitivity factors*  $f_i^s$  to each single argument  $r_i$  with  $i \in [1, I]$

$$F_j^s = F_{\{r_1, r_2, \dots, r_I\}}^s = \prod_{i=1}^I f_i^s(r_i) \quad \forall j \in [1, J], s \in S . \quad (4)$$

Here, the independent sensitivity factors  $f_i^s$  are defined analogous to Eq. (1) using the model forecast

$$q_i^s(r_i, t) := Q_{\{r_{1*}, r_{2*}, \dots, r_{i-1*}, r_i, r_{i+1*}, \dots, r_{I*}\}}^s(t) \text{ where only one argument } r_i \text{ differs from the reference setup}$$

$$f_i^s(r_i) := \frac{1}{T} \sum_{t=t_1}^{t_T} \frac{q_i^s(r_i, t)}{Q_{j_*}^s(t)} \quad \forall i \in [1, I], s \in S . \quad (5)$$

Further, with Eq. (2), every combined sensitivity  $X_j^s$  of implementation  $j$  at position  $s$  is given by

$$X_j^s = X_{\{r_1, r_2, \dots, r_I\}}^s = \ln(F_{\{r_1, r_2, \dots, r_I\}}^s) \stackrel{(4)}{=} \sum_{i=1}^I \ln(f_i^s(r_i)) = \sum_{i=1}^I x_i^s(r_i) , \quad (6)$$

where  $x_i^s(r_i) := \ln(f_i^s(r_i))$  is the *independent sensitivity* referring to a single modified model argument  $i \in [1, I]$  with implementation  $r_i$ . Note that the independent sensitivity factors  $f_i^s(r_i)$  equal one when the implementation  $r_i$  of model argument  $i$  equals the reference implementation  $r_{i*}$  (analogous to Eq. (1)). Consequently, the independent sensitivities  $x_i^s(r_i)$  vanish in Eq. (6) for all  $i$  with  $r_i = r_{i*}$  and each combined sensitivity is given by the sum of independent sensitivities to those arguments, which differ from the reference setup

$$X_j^s = X_{\{r_1, r_2, \dots, r_I\}}^s = \sum_{i=1}^I x_i^s(r_i) \quad \forall j \in [1, J], s \in S . \quad (7)$$

In other words, the assumption of independence implies that the set of all combined sensitivities  $\{X_j^s\}_{j \in [1, J]}$  lies within a  
165 subspace which is spanned by the set of independent sensitivities  $\{x_i^s(r_i)\}_{\substack{r_i \in [1, R_i] \\ i \in [1, I]}}$ . Then, the full set of combined sensitivities  
can be approximated by the subset of independent sensitivities following Eq. (7). This reduces the number of required forecasts  
from  $J_{\text{combi}} = \prod_{i=1}^I R_i$  to:

$$J_{\text{indep}} = 1 + \sum_{i=1}^I (R_i - 1) \quad , \quad (8)$$

with  $J_{\text{indep}} \ll J_{\text{combi}} = J$  as shown in Fig. 1. Therewith, the independent method requires a significantly reduced number of  
170 simulations, one for the reference setup ( $r_{i*} = 1 \forall i$ ) and one for each other implementation  $r_i \in [2, R_i]$  of each argument  
 $i \in [1, I]$ . For example, considering  $I = 3$  model arguments with  $R_i = 5$  implementations each, the total number of  $J_{\text{combi}} = 5^3 = 125$  combined sensitivities reduces to  $J_{\text{indep}} = 1 + 3 \cdot 4 = 13$  independent sensitivities. For  $I = 10$  model arguments  
with  $R_i = 2$  implementations each, the number of required sensitivities can even be reduced by two orders of magnitude  
( $J_{\text{indep}} = 11$ ,  $J_{\text{combi}} = 1024$ ). While the number of required simulations is considerably reduced, the underlying assumption of  
175 independent sensitivities disregards nonlinear interactions between different model arguments. A discussion of this assumption  
for the application to atmospheric model parameters is given in Sect. 5.

### 3 Algorithm

This section provides the description of the ensemble generation algorithm with respect to correlated model parameters. Here,  
a model parameter may be any parameter in the prognostic equations of the model state variables (compare Sect. 2.1). Making  
180 use of the Karhunen-Loéve (KL) expansion, the approach is denoted as *KL ensemble generation approach* thereafter. It is based  
on the fact that the forecast model acts as a dynamical system forcing spatial and multivariate couplings of the atmospheric  
state. Thus, information on the size and coupling of forecast uncertainties can be extracted from differently configured model  
simulations. The configurations of the model simulations is selected by the user according to sources of uncertainties of the  
selected model parameters. For recurring applications of the ensemble generation algorithm, the selection may also be guided  
185 by results of previous applications of the algorithm

The explicit algorithm presented here focuses on state-dependent model parameters which depend on the specific model  
setup. Generally, atmospheric models are sensitive to their specific simulation setup including a large variety of model inputs  
and configurations like initial and boundary conditions, external input data and the selection of parameterization schemes  
in the model. Although comprising a highly heterogeneous set, all model inputs and configurations determining the specific  
190 simulation setup are henceforth denoted as model arguments. For state-dependent parameters considered here, their sensitivities  
to the model setup are assumed to induce dominant uncertainties. Thus, the problem of estimating multivariate uncertainties is  
transferred to sensitivities to the model setup.

The algorithm consists of three major steps which are described in the following: the construction of parameter covariances  
from combined or independent sensitivities (Sect. 3.1), the extraction of leading uncertainties using a highly-parallelized eigen-

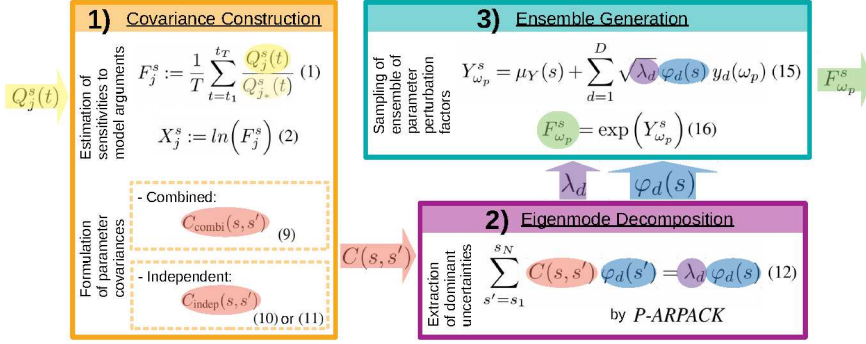


**Figure 2.** Simplified schematic overview of the KL ensemble generation algorithm. Equation numbers refer to the equations in Sect. 2 and Sect. 3. Colored arrows indicate input and output of the algorithm as well as transfer of selected fields between the single steps.

195 mode decomposition software (Sect. 3.2), and the ensemble generation by sampling perturbations from leading eigenmodes with the Karhunen-Loéve expansion (Sect. 3.3). A graphical overview of the major steps composing the algorithm is given in Fig. 2. The formulation of the algorithm is based on the concept of sensitivity estimation introduced in Sect. 2, an overview over the terms used in this section is given in Tab. 1.

### 3.1 Covariance Construction

200 As a first step, essential uncertainties of the model parameters are formulated as multivariate covariance matrix  $C \in \mathcal{R}^{N \times N}$ , where  $N$  is the dimension of the problem i.e. the total dimension of the set of considered model parameters. Generally, the covariances may be determined from any kinds of uncertainties like statistical model errors derived from operational forecasts. Because this study focuses on state-dependent parameters, essential uncertainties are estimated from sensitivities of those parameters to different model arguments. These state-dependent sensitivities are realized as temporally-averaged sensitivity 205 factors with respect to a selected reference as described in Sect. 2. The temporal averaging makes the sensitivities being representative for a sufficient time interval for ensemble simulation.

Generally, the covariance matrix should represent the complete set of essential uncertainties of the model parameters. Focusing on uncertainties induced by sensitivities to various model arguments  $i \in [1, I]$ , essential uncertainties can be estimated from different implementations  $r_i$  of each model argument  $i$ . Ideally, the covariance matrix is calculated from the sensitivities 210  $\{X_j^s\}_{j \in [1, J]}$  to all possible combinations of various implementations of each argument (compare Sect 2.2). In this case, the *combined covariance* between sensitivities at positions  $s, s' \in S$  is given by

$$C_{\text{combi}}(s, s') := \frac{1}{J-1} \sum_{j=1}^J \left( (X_j^s - \mu_{\text{combi}}(s)) \cdot (X_j^{s'} - \mu_{\text{combi}}(s')) \right) , \quad (9a)$$

$$\text{where } \mu_{\text{combi}}(\tilde{s}) := \frac{1}{J} \sum_{j=1}^J X_j^{\tilde{s}} \quad | \quad \tilde{s} = s, s' \quad (9b)$$

is the mean value of combined sensitivities at position  $s$  and  $s'$ , respectively.

215 If the assumption of independent sensitivities is applied, covariances are calculated from the set of independent sensitivities  $\left\{x_i^s(r_i)\right\}_{\substack{r_i \in [1, R_i] \\ i \in [1, I]}}$  (compare Sect. 2.3). Rather than approximating all combined sensitivities from independent sensitivities explicitly, the effects on mean sensitivities and covariances are derived in its general form in Appendix A. In the KL ensemble generation algorithm, the mean values  $\mu_{\text{indep}}(s)$  and covariances  $C_{\text{indep}}(s, s')$  of the sensitivities are directly calculated from the set of independent sensitivities by

$$220 \quad \mu_{\text{indep}}(s) \stackrel{(A3)}{=} \sum_{i=1}^I \left( \frac{1}{R_i} \cdot \sum_{r_i=1}^{R_i} x_i^s(r_i) \right) \stackrel{(7)}{=} \sum_{i=1}^I \left( \frac{1}{R_i} \cdot \sum_{\substack{r_i=1 \\ r_i \neq r_{i*}}}^{R_i} x_i^s(r_i) \right) , \quad (10a)$$

$$\begin{aligned} C_{\text{indep}}(s, s') &\stackrel{(A4)}{=} \frac{J}{J-1} \sum_{i=1}^I \left[ \left( \frac{1}{R_i} - \frac{1}{(R_i)^2} \right) \cdot \sum_{r_i=1}^{R_i} (x_i^s(r_i) \cdot x_i^{s'}(r_i)) \right] \\ &\stackrel{(7)}{=} \frac{J}{J-1} \sum_{i=1}^I \left[ \left( \frac{1}{R_i} - \frac{1}{(R_i)^2} \right) \cdot \sum_{\substack{r_i=1 \\ r_i \neq r_{i*}}}^{R_i} (x_i^s(r_i) \cdot x_i^{s'}(r_i)) \right] . \end{aligned} \quad (10b)$$

Note that the assumption of independence does not imply orthogonality between the input sensitivities. While the equations are exact under the given assumption of tangent-linearity, this assumption might be a strong limitation for many atmospheric processes.

225 The method of independent sensitivities allows the inclusion of additional uncertainties in a straightforward way. These additional uncertainties may originate from any other error source not represented as model arguments. For example, this could be a known uncertainty in the formulation of the model itself. If such an *additional uncertainty* is given (e.g. from statistical evaluation), it can be included as additional sensitivity  $x_{\text{add}}^s$  with  $R_{\text{add}} = 2$ . Based on Eq. (10), the independent mean and covariance including additional uncertainties are

$$230 \quad \mu_{\text{indep}}^{\text{add}}(s) = \sum_{i=1}^I \left( \frac{1}{R_i} \cdot \sum_{\substack{r_i=1 \\ r_i \neq r_{i*}}}^{R_i} x_i^s(r_i) \right) + \frac{1}{R_{\text{add}}} \cdot x_{\text{add}}^s , \quad (11a)$$

$$C_{\text{indep}}^{\text{add}}(s, s') = \frac{J}{J-1} \left( \sum_{i=1}^I \left[ \left( \frac{1}{R_i} - \frac{1}{(R_i)^2} \right) \cdot \sum_{\substack{r_i=1 \\ r_i \neq r_{i*}}}^{R_i} (x_i^s(r_i) \cdot x_i^{s'}(r_i)) \right] + \frac{1}{(R_{\text{add}})^2} \cdot (x_{\text{add}}^s \cdot x_{\text{add}}^{s'}) \right) . \quad (11b)$$

If the direction of the additional uncertainty is unknown (*unsigned additional uncertainty*), the original definition of the mean values for independent sensitivities as given in Eq. (10a) is used instead of Eq. (11a). This ensures no impact of the additional uncertainty to the mean values of the parameters.

### 3.2 Eigenmode Decomposition

Once the multivariate covariances are formulated, dominating directions of uncertainties are extracted as second step. This extraction is realized by an eigenmode decomposition of the covariance matrix

$$\sum_{s'=s_1}^{s_N} C(s, s') \varphi_d(s') = \lambda_d \varphi_d(s) , \quad (12)$$

with  $\lambda_d$  the  $d$ -th eigenvalue and  $\varphi_d(\tilde{s})$  the  $\tilde{s}$ -th element of the corresponding eigenvector  $\varphi_d \in \mathcal{R}^N$  for all  $d \in [1, N]$  with  $\tilde{s} = s, s' \in S$ . As the presented approach focuses on dominant uncertainties, the  $D$  largest eigenvalues and corresponding eigenvectors are required  $\lambda_1 \geq \lambda_2 \geq \dots \geq \lambda_D$  with  $D < N$ . Here, the first eigenvalues represent the size of the most dominant uncertainties and the corresponding eigenvectors their directions. Due to the high-dimensionality of atmospheric models, the covariance matrix may easily be of the order of  $10^{10}$  elements. This inhibits explicit storage of the matrix and makes the computation of the eigenproblem Eq. (12) very costly even for a low number of required eigenmodes ( $D \ll N$ ). Therefore, a highly efficient software is required which is suitable for high-dimensional systems.

The ARPACK (ARNoldi PACKage, Lehoucq et al., 1997) package is a flexible tool for numerical eigen and singular value decomposition. It is explicitly developed for large-scale problems and includes a set of specific algorithms for different types of matrices. The ARPACK software uses a reverse communication interface where the matrix needs to be given as operator acting on a given vector. APRACK makes use of the Implicitly Restarted Arnoldi Method (IRAM, Sorensen, 1997) which is based on the implicitly shifted QR-algorithm. As a covariance matrix is quadratic, symmetric and positive definite by construction, the IRAM method reduces to the Implicitly Restarted Lanczos Method (IRLM). In this study, the parallel version P-ARPACK is used for the eigenmode decomposition, which balances the workload of processors and reduces the computation time. For a detailed description of the ARPACK software package see Lehoucq et al. (1997).

### 255 3.3 Ensemble Generation

The final step is the generation of an ensemble of perturbations based on the leading eigenmodes of parameter uncertainties. This step makes use of the Karhunen-Loéve expansion – denoted as *KL expansion* thereafter – named after Karhunen (1947) and Loéve (1948). The KL expansion provides a mathematically optimal combination of the dominant directions of parameter uncertainties given by the leading eigenmodes. The following description is adopted from the notations of Schwab and Todor (2006) and Xiu (2010), to which the reader is referred for more details. In its discrete form, the KL expansion describes the  $s$ -th element of a stochastic process  $Y_{\omega_p}^s$  of dimension  $N$  as linear combination of orthogonal components

$$Y_{\omega_p}^s = \mu(s) + \sum_{d=1}^N \psi_d(s) y_d(\omega_p) , \quad (13)$$

with  $\mu(s)$  denoting the mean value of the stochastic process and  $\omega_p$  its  $p$ -th random realization. Here, the deterministic fields  $\psi_d(s)$  are given by the eigenvalues  $\lambda_d$  and eigenvectors  $\varphi_d$  of the covariances of the stochastic process

$$265 \quad \psi_d(s) := \sqrt{\lambda_d} \varphi_d(s) \quad (14)$$

In this notation, the stochastic coefficients  $y_d(\omega_p)$  are independent random numbers with zero mean and unit standard deviation.

In the context of ensemble generation, the stochastic process is a set of *perturbations*  $\{Y_{\omega_p}^s\}_{s \in S}$  whose essential uncertainties are formulated as covariance matrix of the sensitivities as defined in Sect. 3.1. Thus, the eigenvalues  $\lambda_d$  and corresponding normalized eigenvectors  $\varphi_d(s)$  are provided by the eigenmode decomposition in Sect. 3.2. Normally distributed sensitivities 270  $X_j^s$  can be realized by centered and normally distributed stochastic coefficients  $y_d(\omega_p)$ .

Using the KL expansion for ensemble generation, multivariate covariances induce coupled perturbations of the set of considered parameters. The higher the correlations of the sensitivities, the faster is the decrease of the eigenmodes and the more are the perturbations determined by a few leading orthogonal components. Truncating Eq. (13) at  $D < N$ , the resulting KL approximation provides an optimal approximation of the stochastic process in the least-square sense (Schwab and Todor, 2006).

275 For ensemble generation, a set of  $D$  stochastic coefficients  $\{y_d(\omega_p)\}_{d \in [1, D]}$  is randomly sampled for each ensemble member  $p$  from a normal distribution with zero mean and unit standard deviation. Given the set of leading eigenvalues  $\{\lambda_d\}_{d \in [1, D]}$  and corresponding normalized eigenvectors  $\{\varphi_d(s)\}_{d \in [1, D], s \in S}$ , the perturbation of ensemble member  $p \in [1, P]$  at position  $s \in S$  is sampled from

$$Y_{\omega_p}^s = \mu_Y(s) + \sum_{d=1}^D \sqrt{\lambda_d} \varphi_d(s) y_d(\omega_p) \quad \forall \omega_p \in [\omega_1, \omega_P], s \in S. \quad (15)$$

280 Finally, the ensemble of perturbations is transferred back to a set of *perturbation factors*  $\{F_{\omega_p}^s\}_{s \in S}$ . If the model parameters are assumed to be lognormally distributed, a resubstitution as counterpart of the logarithmic substitution in Eq. (2) is performed

$$F_{\omega_p}^s = \exp(Y_{\omega_p}^s) \quad \forall \omega_p \in [\omega_1, \omega_P], s \in S. \quad (16)$$

These perturbation factors will then be applied to the model parameters in the ensemble forecast.

285 Using the KL expansion for ensemble generation instead of singular vectors has one important advantage. In SV based ensemble generation approaches, each perturbation is generated by one singular vector scaled by its singular value. Using the KL expansion, each perturbation is sampled from the series of eigenmodes using different random numbers for each perturbations. This allows for a flexible selection of the number of perturbations depending on the desired level of detail. Independent of the number of perturbations, the KL expansions ensures an optimal estimation of the largest uncertainties by 290 the calculated perturbations.

## 4 Application to Biogenic Emissions

This section provides results of the KL ensemble generation algorithm for an application to biogenic emissions in a regional CTM system. The modeling system used for the calculation of sensitivities and the specific setup of the algorithm are described in Sect. 4.1 and Sect. 4.2, respectively. Based on these, the results are presented with respect to two main objectives: Firstly, 295 the behavior of the algorithm is illustrated for two different setups using combined and independent sensitivities, respectively.

Sect. 4.3-4.5 present the results for each of the three major steps of the algorithm as described in Sect. 3. The description focuses on similarities between the two methods rather than on the detailed description of specific patterns. For the setup of independent sensitivities, additional uncertainties are included as described in Sect. 4.2 to demonstrate the inclusion of those. Secondly, the performance of the algorithm is evaluated for the two different setups. A comprehensive a-posteriori evaluation would ideally be based on a representative amount of data covering multiple conditions. However, observations of biogenic gases are rare and do only provide information on local concentrations, not on their emissions itself. As concentrations are affected by other uncertain processes, an ensemble of emissions or emission factors produced by the algorithm cannot be evaluated by observations alone. Therefore, Sect. 4.6 evaluates the performance of the algorithm in terms of ensemble statistics.

#### 4.1 Modeling System

The KL ensemble generation algorithm was implemented in a way that it uses precalculated output from the EURAD-IM (*EUROpean Air pollution Dispersion - Inverse Model*) chemical data assimilation system. Note that the algorithm is independent of the forecast model, which can be replaced by any other CTM. EURAD-IM combines a state-of-the-art chemistry transport model (CTM) with 4-dimensional variational data assimilation (Elbern et al., 2007). Based on meteorological fields precalculated by WRF-ARW (*Weather Research and Forecasting - Advanced Research WRF*, Skamarock et al., 2008), the Eulerian CTM performs forecasts of about 100 gas phase and aerosol compounds up to lower stratospheric levels. In addition to advection and diffusion processes, modifications due to chemical conversions are considered by the RACM-MIM chemical mechanism (*Regional Atmospheric Chemistry Mechanism - Mainz Isoprene Mechanism*, Pöschl et al., 2000; Geiger et al., 2003). Emissions from anthropogenic and biogenic sources as well as dry and wet deposition act as chemical sources and sinks, respectively. In this study, the EURAD-IM system provides forecasts of sensitivities to various model arguments, which are used for covariance construction in the KL algorithm. The concept of emission factors used for emission rate optimization in EURAD-IM was adapted in the KL ensemble generation approach as described below.

The KL ensemble generation algorithm is tested for biogenic emissions which are known to be subject to large uncertainties. The MEGAN 2.1 model developed by Guenther et al. (2012) calculates biogenic emissions of various compounds in EURAD-IM as function of atmospheric and terrestrial conditions including radiation, air temperature, leaf area index, and soil moisture. In this study, biogenic emissions of five dominant volatile organic compounds (VOC) are perturbed: isoprene, limonene, alpha-pinene, ethene, and aldehydes. Note that biogenic aldehyde emissions from MEGAN 2.1 represent the total emission from acetaldehyde and a set of higher aldehydes which are not treated individually (see Guenther et al., 2012, for further details). Due to a collective approach in MEGAN 2.1, the biogenic emissions of different compounds are assumed to be highly correlated. Thus, the set of five biogenic emission fields is selected in order to investigate the joint perturbation of highly uncertain, yet correlated parameters. In the KL algorithm, sensitivities from the five emission fields induce multivariate covariances in the covariance matrix  $C$  which allow for joint perturbation of those. The following description of the results focuses on emissions of isoprene, which is the most abundantly emitted biogenic trace gas.

## 4.2 Setup

In the KL algorithm, sensitivities used for covariance construction are taken from a case study covering the Po valley in northern Italy on 12.07.2012. A preceding study by Vogel and Elbern (2021a) demonstrated that local emissions of biogenic volatile organic compounds (BVOCs) are highly sensitive to various model arguments during this case study. At the same time, these sensitivities are found to be almost species invariant and show little variation on an hourly timescale which allows for a generalized formulation of perturbations. Providing an appropriate test case, the sensitivities used in this study are based on the results of Vogel and Elbern (2021a) which have been simulated by EURAD-IM.

Specifically, emission sensitivity factors  $F_j^s$  are calculated from hourly biogenic emissions divided by the corresponding reference emissions and averaged over the period on 12.07.2012 from 00 UTC until 10 UTC according to Eq. (1). Here, minimum emissions of  $1.0 \cdot 10^{-3} \frac{kg}{km^2 h}$  are defined and sensitivity factors are limited by 0.1 and 10.0 in order to avoid unrealistic perturbations in regions of low emissions. As biogenic emissions are restricted to terrestrial vegetation, only land surface gridboxes are used, which reduces the total dimension of the problem by about 27 % compared to all surface gridboxes.

Two different implementations are selected for each argument ( $R_i = 2, \forall i \in [1, 6]$ ), where the reference  $r_{i*} = 1, \forall i$  is the default configuration of EURAD-IM and  $r_i = 2$  are the alternative implementations of each argument  $i$ . Figure 3 shows 32 combined sensitivity factors of biogenic emissions calculated from EURAD-IM using Eq. (1) with different combinations of model configurations as listed in Tab. B1. For computational reasons, the subset of  $J_{combi} = 32$  combined sensitivities is sampled from a total number of  $J = 2^6 = 64$  possible combinations. (A detailed discussion of the origin of sensitivity factors used in this study is given in Vogel and Elbern (2021a). The selection of 32 combined configurations is based on the importance of the source of uncertainties reported there.)

In contrast to the large amount of calculations required for combined sensitivities, the method of independent sensitivities is additionally investigated. As described in Sect. 2.3, only sensitivities resulting from the change of a single model argument are required for this method. This allows for an additional consideration of two uncertainties related to the emission model. These uncertainties are selected to demonstrate the inclusion of additional uncertainties in order to provide a most realistic setup of the ensemble for biogenic emissions. Firstly, the highly variable response of biogenic emissions to soil dryness is added to the set of independent sensitivities. This sensitivity is defined as the change of emissions when the drought response used in MEGAN2.1 is excluded (compare Vogel and Elbern, 2021a). Secondly, Guenther et al. (2012) indicate an uncertainty of the emissions model itself of 200 %, which is included as unsigned additional uncertainty (denoted as *a-priori uncertainty*) with a constant factor of two for all locations and trace gases. Note that an unsigned additional uncertainty does only apply to the covariances given by Eq. (11b) and does not affect the calculation of the independent mean given by Eq. (10a). The formulation of a constant factor induces a simple assumption representing perfectly correlated errors in this case. But it is assumed to be sufficient to show the effect of including unsigned additional uncertainties in the algorithm.

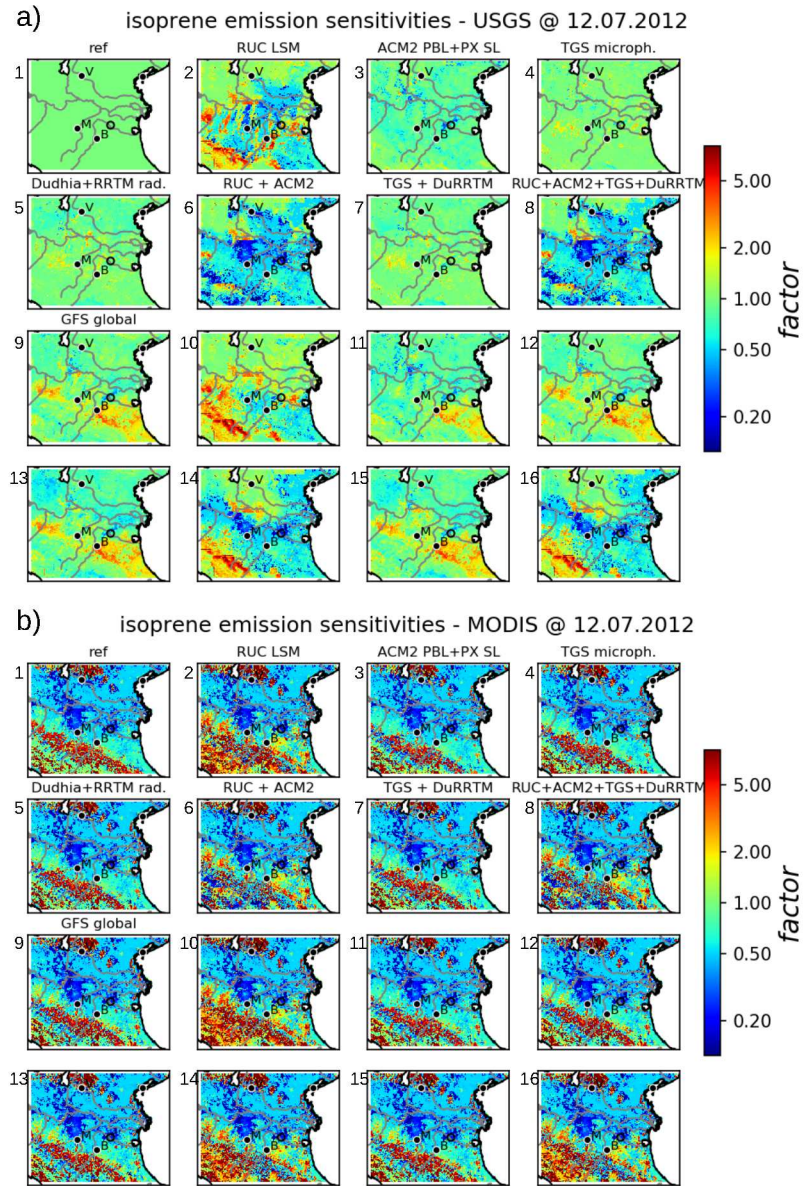


**Figure 3.** Set of combined sensitivities of isoprene emissions. Shown are isoprene emission factors for different combinations of model arguments as simulated by EURAD-IM. Emission factors are temporally averaged ratios of emissions divided by the reference emissions. The specific setup used for each of the 32 sensitivities given in Tab. B1. The sensitivities are divided into those using USGS (a) and MODIS (b) land use information, numbers attached to the individual subplots refer to the numbers in Tab. B1. In addition, a short abbreviation of the setup is given above each subplot. See also Vogel and Elbern (2021a) for a detailed description of the abbreviations and model implementations. Some major cities (Verona, Bologna, Modena) are indicated by their initial letters.

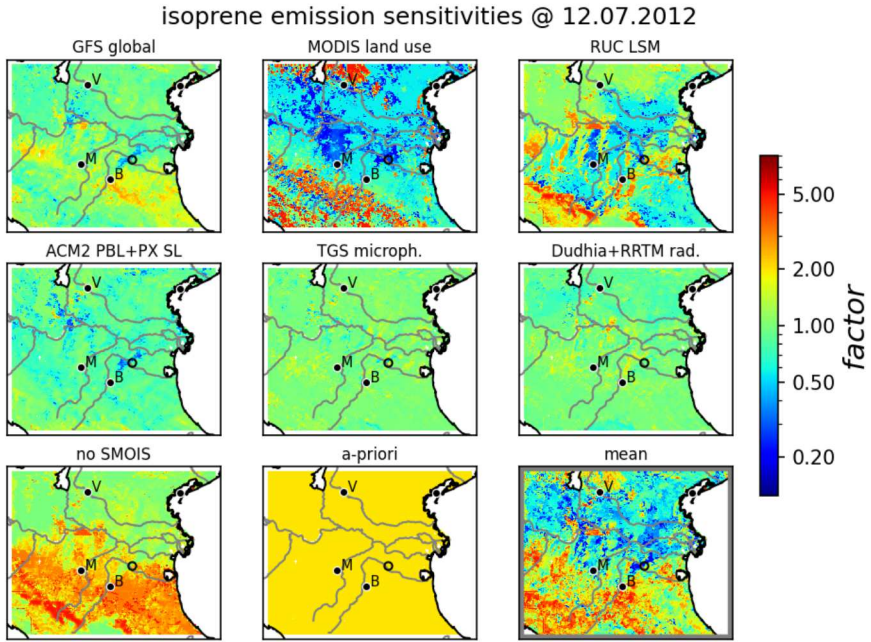


**Figure 4.** Set of independent sensitivities of isoprene emissions simulated by EURAD-IM. Shown are isoprene emission factors of simulations where only one model argument differs from the reference setup. Plotting conventions including abbreviations as in Fig. 3. Additional uncertainties refer to the drought response ('no SMOIS') and the emission model ('a-priori') of biogenic emissions. The lower right subplot shows the independent mean from these sensitivities using Eq. (10a). A detailed description of the abbreviations and model implementations is provided by Vogel and Elbern (2021a).

#### 4.3 Sensitivity Estimation

According to the definition in Eq. (1), sensitivity factors of the reference run (subplot 1 of Fig. 3a) are equal to 1 by definition. The set combined sensitivities is dominated by effects of land use information shown in Fig. 3b, inducing reduced or increased emissions in the mountains and the Po valley, respectively. As discussed in Vogel and Elbern (2021a), these large sensitivities in biogenic emissions are caused by different fractions of broadleaf trees in USGS land use information and MODIS data. Significant effects are also found with respect to global meteorology, land surface model (LSM) and boundary layer schemes. Here, weak nonlinear effects appear when RUC LSM is combined with the ACM2 boundary layer scheme or GFS global meteorology (subplot 6 and 10 of Fig. 3a).

Figure 4 shows the independent mean factors and sensitivities for isoprene emissions. Note that independent sensitivities are formulated relative to the independent mean, which are both limited by 0.2 and 5 to be consistent with the configuration for combined sensitivities. Similar to the results of combined sensitivities, MODIS land use information and RUC land surface model produce significantly reduced isoprene emissions within the northern Po valley. The added sensitivity to drought

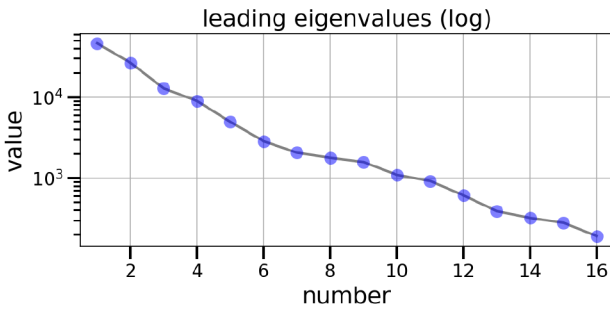


**Figure 5.** Leading eigenvalues of biogenic emissions for combined sensitivities (blue dots). Eigenvalues are plotted on a logarithmic scale.

response points towards increased emissions in the southern part of the domain. Consequently, the independent mean is dominated by reduced emissions in the northern part and increased values in the southern part. The a-priori uncertainty of the emission model is represented by a constant factor of two and does not affect the independent mean by definition. The remaining independent sensitivities produce only minor deviations in biogenic emissions of all trace gases including isoprene.

#### 375 4.4 Eigenmode Decomposition

Based on the respective formulation of combined or independent sensitivities, the leading eigenvalues and their associated eigenvectors of the covariance matrices are calculated as described in Sect. 3.2. For combined sensitivities, the eigenvalues given in Fig. 5 show a logarithmic decrease of about one order of magnitude within the first five modes. This indicates that the major uncertainties of the emissions factors are determined by a few leading directions. In other words, the fast decrease 380 of leading eigenvalues confirms a high correlation of biogenic emissions through the domain and between different gases. The contribution of these leading eigenmodes to local emission factors for each trace gas is given by the corresponding eigenvectors shown in Fig. 6. According to shape and size of the first eigenmode, it is almost exclusively induced by the sensitivity to land use information which is invariant to the other sensitivities. The subsequent eigenmodes represent common patterns of the remaining sensitivities which are therefore treated together.

385 As for combined sensitivities, the eigenmode decomposition extracts perpendicular components from the set of independent sensitivities. The eigenvalues shown in Fig. 7 state a similar decrease of eigenvalues for independent sensitivities compared to the combined method. Highly similar size and decrease rate of leading eigenvalues indicate a reasonable representation of the leading uncertainties by the independent method. However, nonlinearities arising from combined changes in the land surface model with global meteorology or boundary layer schemes are not captured by the linear assumption of independent 390 sensitivities.

According to the corresponding eigenvectors in Fig. 8, the first eigenmode represents common features of the a-priori uncertainty and the other independent sensitivities. While the second eigenmode is closely related to the effects of drought response and the land surface model, the sensitivity to land use dominates the third eigenmode. Besides that, highly similar signals in eigenvectors for different biogenic gases state a considerably large correlation between those. Yet, individual patterns

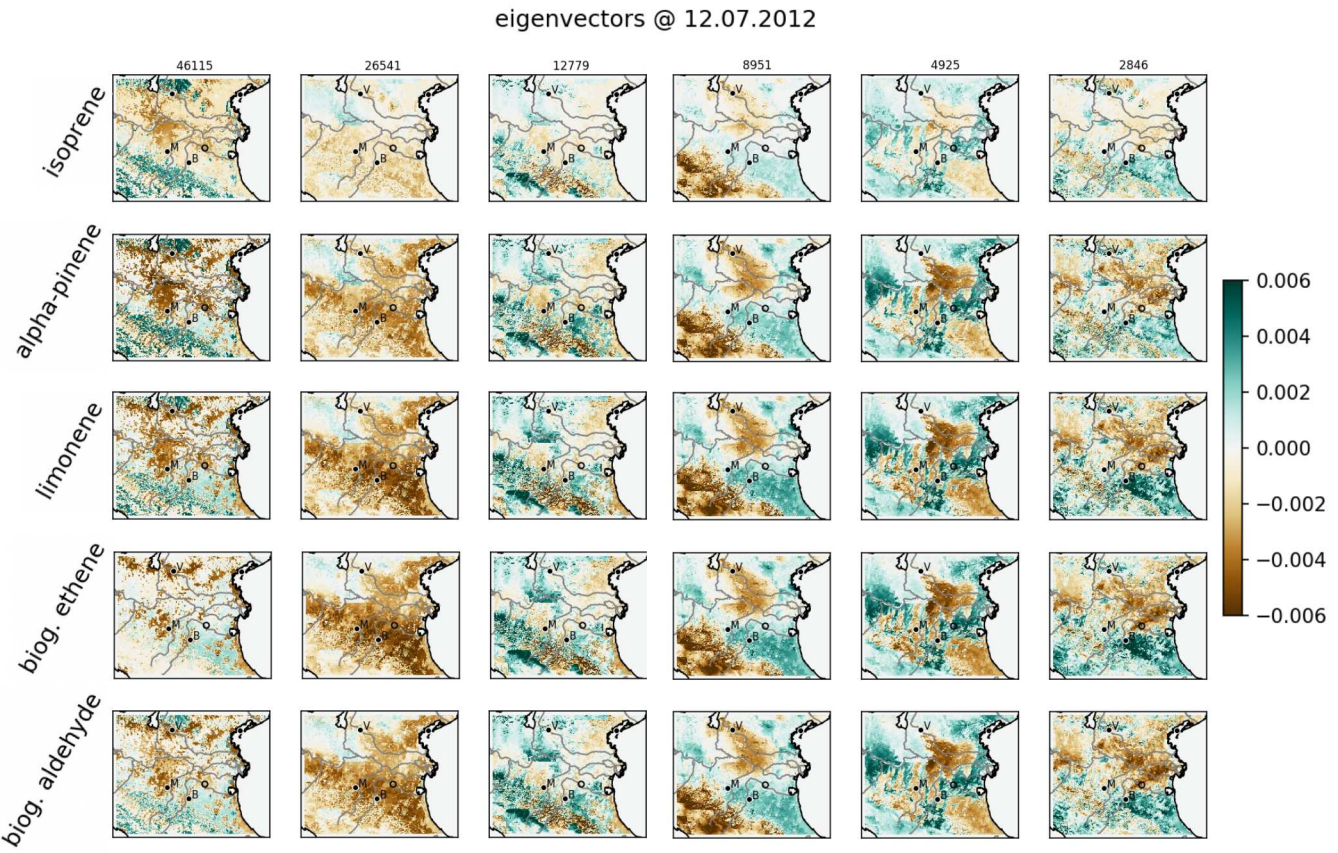


**Figure 6.** Leading eigenvectors for combined sensitivities. The normalized eigenvectors are visualized as column of fields of different biogenic gases. Numbers above each column show the eigenvalues of the corresponding eigenvector.

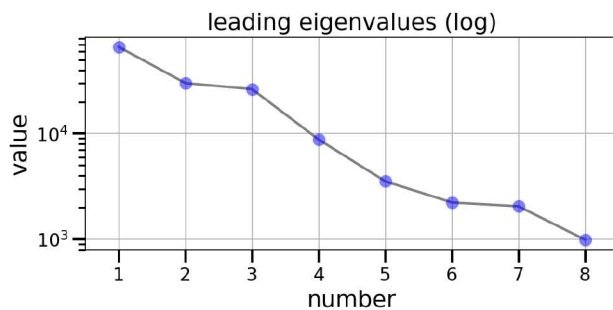


**Figure 7.** Leading eigenvalues of biogenic emissions for independent sensitivities including additional uncertainties. Plotting conventions as in Fig. 5.

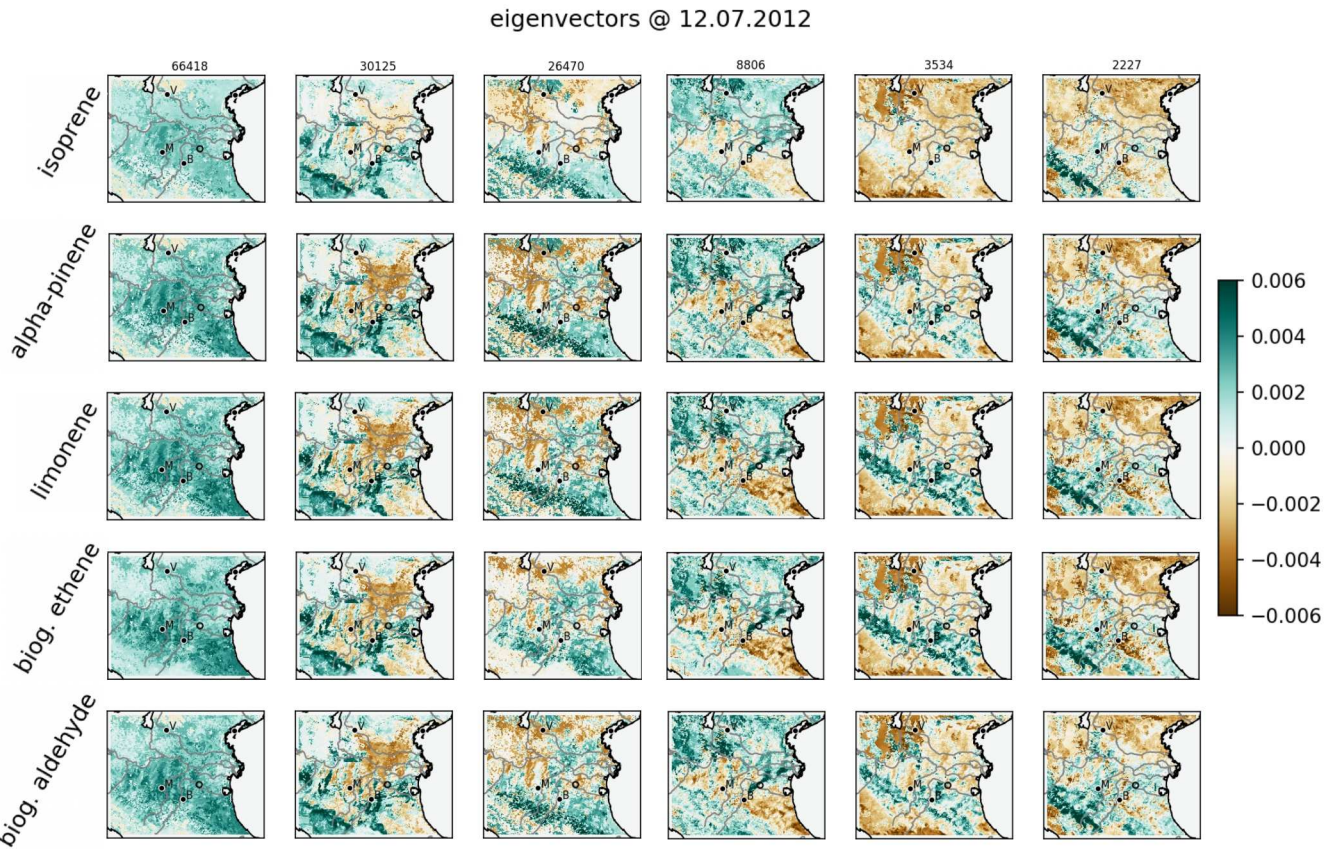


**Figure 8.** Leading eigenvectors for independent sensitivities including additional uncertainties. Plotting conventions as in Fig. 6.

395 of each biogenic gas are also represented by the leading eigenmodes for independent sensitivities. These patterns are also found for the eigenvectors of combined sensitivities (compare Fig. 6) which confirms the suitability of the independent method with respect to multiple parameters. Note that the consideration of additional uncertainties in the independent method does not allow for a direct comparison of individual eigenmodes.

#### 4.5 Ensemble Generation

400 The different setups of the covariances from combined and independent sensitivities prohibit a direct comparison of their perturbations. As the ensemble generation from leading eigenmodes does not differ between these two setups (compare Sect. 3.3), resulting perturbations are only shown for independent sensitivities.

Figure 9 displays eight realizations of perturbations in terms of emission factors for isoprene for independent sensitivities. The perturbation factors of all biogenic emissions are calculated by multiplying the independent mean factors of the sensitivities 405 with different realizations of the KL expansion. As the KL expansion does not affect the mean values, ensemble mean emission factors remain similar to the one of the sensitivities (compare Fig. 4). Although differences in perturbation factors are large, this

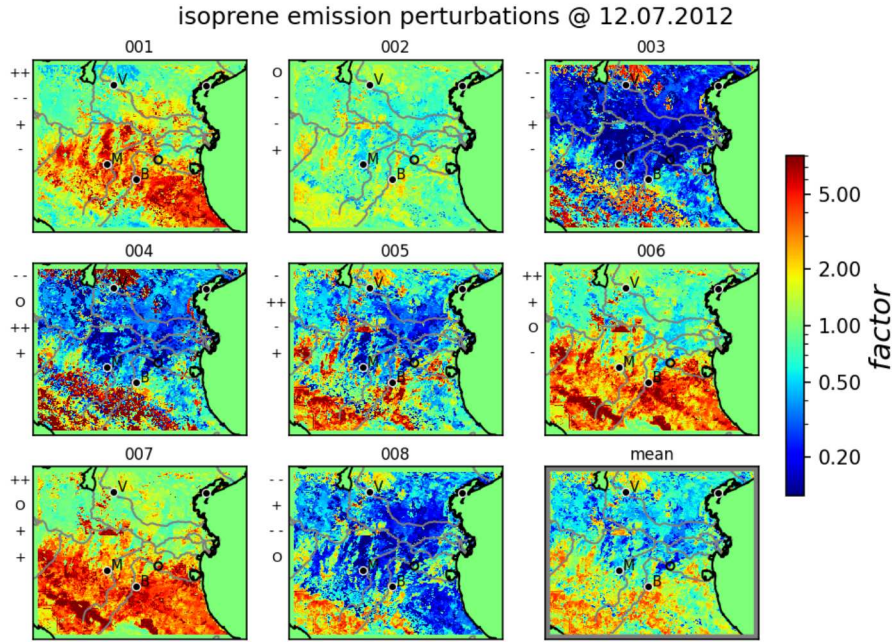


**Figure 9.** Perturbations of isoprene emissions for independent sensitivities including additional uncertainties given as factors w.r.t reference emissions. Random realizations of stochastic coefficients for the leading eigenmodes of each member are indicated left of each subplot ( '++': large positive value ( $> 1.$ ), '+': small positive value ( $0.1 < * < 1.$ ), 'O': very small absolute value ( $-0.1 < * < 0.1$ ), '-': small negative value ( $-1. < * < -0.1$ ), '--': large negative value ( $< -1.$ ) ). The lower right subplot gives the ensemble mean factors. Some major cities (Verona, Bologna, Modena) are indicated by their initial letters.

suggests a reasonable sampling of the eight realizations. Concerning the individual members, the high number of significant uncertainties results in emission factors ranging up to more than one order of magnitude. Each realization is influenced by different combinations of the leading eigenmodes resulting in different perturbation patterns. While realization 001, 006 and  
410 007 are dominated by a positive contribution of the first eigenmode, the effect of the second mode is clearly visible when comparing realization 001 and 006. Comparing realization 004 and 008, the most significant differences are induced by the third eigenmode. Due to the fast decrease of eigenmodes, comparably small contributions of the remaining modes remain invisible in the perturbation factors. Thus, the comprised KL ensemble is restricted to dominant uncertainties indicated by the leading eigenmodes. In this case, these uncertainties are mainly induced by sensitivities to various surface conditions, which is  
415 in accordance to Vogel and Elbern (2021a).

#### 4.6 Ensemble Evaluation

The performance of the KL ensemble perturbations is evaluated by ensemble statistics. Note that this evaluation does only relate to the algorithm itself - i.e. how well the algorithm is able to capture the uncertainties indicated by the sensitivities.

The question on how well the sensitivities represent the true parameter uncertainties is not part of the evaluation and beyond  
420 the scope of this study. In order to be able to compare the statistics of the KL ensembles using combined and independent  
sensitivities,  $I = 6$  model arguments are considered for both setups. While the setup of 32 combined sensitivities is the same  
as in the previous sections ( $J_{combi} = 32$ ), no additional uncertainties were included in the independent setup ( $J_{indep} = 7$ ).  
Despite this, the setup remains as described in Sect. 4.2.

In Fig. 10, statistics of the ensemble perturbation factors from the KL algorithm with combined sensitivities are compared  
425 to statistics of the sensitivity factors from 32 combined sensitivities. Because these 32 combined sensitivities serve as input  
for the algorithm in the combined method, the ensemble statistics at all locations should ideally coincide with the identity  
line. Thus, deviations from the identity line give an indication of the sampling error induced by the limited number of used  
eigenmodes and the low number of 8 realizations compared to the dimension of the problem. Mean isoprene emission factors  
for the combined method are well represented by the KL algorithm, deviations remain below 20% for almost all locations  
430 (Fig. 10a).

Ensemble standard deviations show more significant deviations (Fig. 10b). For low and medium values, standard deviations  
of the KL ensemble with combined sensitivities range from 75% until 130% of the respective input values. This almost  
homogeneous scatter around the input values is likely induced by minor uncertainties which are not captured by the leading  
eigenmodes. At some locations, the KL ensemble produces a set of high standard deviations between 5.0 and 8.0 which are not  
435 found in the sensitivities. While the standard deviation is overestimated at these locations, the ensemble mean at these locations  
is slightly underestimated (sensitivities approx. 3.0, combined ensemble perturbations approx. 2.0, Fig. 10a). These deviations  
can be related to the low ensemble size and are expected to reduce for larger ensemble sizes. Additionally, limiting sensitivity  
factors in the KL algorithm may also affect sensitivity statistics in this case (compare Sect 4.2).

The independent method induces larger deviations of mean isoprene emission factors from the mean combined sensitivities.  
440 The increase in deviations mainly represent the additional inaccuracy due to the assumption of independent sensitivities. Note  
that the 32 combined sensitivities used in the evaluation are a subset of 64 possible combinations (compare Sect. 4.2). Because  
the independent method approximates all combinations of sensitivities, some deviations might also relate to the selection of  
the 32 combined sensitivities. Ensemble mean factors correlate well with the combined sensitivities and deviations remain  
between -25% and +50% for most locations (Fig. 10a). While only 7 instead of 32 – or ideally 64 – sensitivities are required  
445 for this setup, the spread of mean mean factors is about twice the spread for the combined ensemble setup.

Deviations of ensemble standard deviations are also slightly increased for the independent method (Fig. 10b). The overesti-  
mation of high standard deviations produced by the combined method is reduced in the independent method. At some locations,  
standard deviations of about 2.0 in the combined sensitivities are underestimated by the KL ensemble with independent sensi-  
tives (standard deviations approx. 1.5). These differences are likely due to nonlinear effects from combining sensitivities which  
450 are neglected in this setup. Nevertheless, the ensemble standard deviations at most locations are well represented by the KL  
ensemble with independent sensitivities.

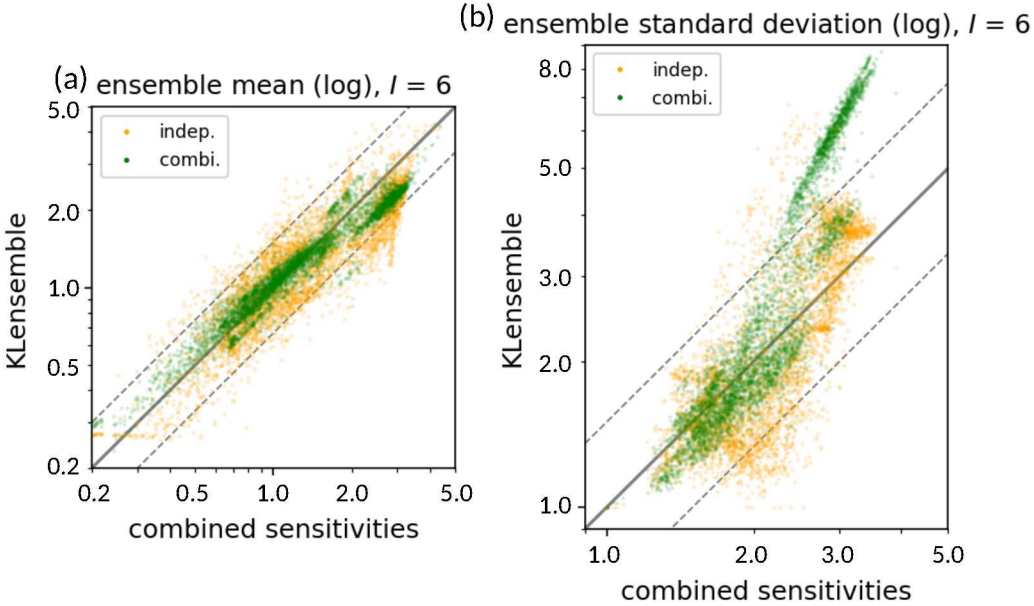


**Figure 10.** Scatter plot of ensemble statistics for isoprene emission perturbations. Shown are logarithmic ensemble mean (a) and standard deviations (b) of the KL ensemble perturbations at each grid-box as function of combined sensitivities. Ensemble statistics are shown for 32 combined (green) and 7 independent (orange) sensitivities, which both refer to the same set of  $I = 6$  considered arguments. The solid gray line indicates the identity line (e.g.  $\mu_{KL} = 1 \cdot \mu_{sens}$  for the ensemble mean) to the set of 32 combined sensitivities, the dashed gray lines represent an over- or underestimation by factor 1.5 (e.g.  $\mu_{KL} = 1.5 \cdot \mu_{sens}$  and  $\mu_{KL} = (1.5)^{-1} \cdot \mu_{sens}$ ).

## 5 Discussion

This section provides a discussion of different aspects regarding the potential and limitations of the KL ensemble generation approach. Concerning the formulation of the algorithm, ensemble perturbations are created from covariances of the stochastic process. The use of the KL expansion ensures that for large ensemble sizes the statistics of the perturbations converge towards their input values determined by the covariances. Consequently, the accuracy of the KL ensemble to represent the true uncertainties crucially relies on the formulation of the covariances. Uncertainties not considered in the formulation of the covariances cannot be captured by the KL ensemble. The major benefit of the approach lies in the optimal properties of the perturbations focusing on leading uncertainties, providing an optimal coverage of uncertainties even for low ensemble sizes.

Although the greatest benefit is achieved for highly correlated parameters, the algorithm is assumed to efficiently combine the major uncertainties even for uncorrelated parameters. In case of missing correlations and therefore lack of ensemble reduction potential, the KL approach retains more leading eigenmodes and does not suppress required degrees of freedom.

By extracting leading eigenmodes from parameter covariances, the problem is transferred to a low-dimensional subspace spanned by the set of leading eigenmodes. This makes the approach highly efficient in covering dominant uncertainties compared to random perturbations at each location. For this uncondensed random approach, perturbations would be sampled from

**Table 2.** Computation time for the solution of the eigenproblem in the KL ensemble generation algorithm for representative setups. The dimension of the system was reduced as described in Sect. 4. The relative computing time is given w.r.t. 8 eigenmodes from 32 combined sensitivities of 5 parameters ("\*"). The last two lines show the setups of independent ("indep") and combined ("combi") sensitivities presented in this study, respectively.

# parameters	sensitivities	# eigenmodes	time	relative time
5	32 (combi)	8	660 sec	*
1	32 (combi)	8	22 sec	0.03
5	8 (combi)	8	122 sec	0.18
5	8 (indep)	8	148 sec	0.22
5	32 (combi)	16	1108 sec	1.68

"# parameters" = number of different model parameters considered, "sensitivities" = number and type of sensitivities used for covariance construction, "# eigenmodes" = number of eigenvalues and -vectors calculated, time = physical time required for computation of perturbations, relative time = computation time divided by reference computation time

the complete  $N$ -dimensional space given by all considered model parameters at all grid-boxes. Compared to the uncondensed approach, the sampling space from which the KL perturbations are sampled is reduced to a  $D$ -dimensional eigenmode subspace. The higher the parameter correlations, the less eigenmodes need to be considered in order to obtain sufficient sampling of uncertainties. Most atmospheric chemical parameters have high spatial- and cross-parameter-correlations which enables  
 470  $D \ll N$  and thus significant reduction of the sampling space. In the results presented in this study, this has been demonstrated for a set of biogenic emissions with dimension  $2 \cdot 10^6$ . In this case, that sampling about 10 ensemble members from the leading eigenmodes is sufficient to cover the leading uncertainties of the high-dimensional parameters. The required numbers of eigenmodes and ensemble perturbations depend on the desired level of detail of the ensemble. Independent of the level of detail, the KL expansions ensures an optimal estimation of covariances by the calculated perturbations.

475 Once the sensitivities are calculated, the computational effort required for the generation of Karhunen-Loéve (KL) perturbations is mainly consumed by the numerical solution of the eigenproblem. The highly efficient parallelization of the solution of the eigenproblem by parallel-ARPACK renders the algorithm suitable for high-dimensional systems. Table 2 summarizes the computation time and relevant properties for selected setups. By definition, the computing time is proportional to the size of the covariance matrix, which increases quadratically with the dimension of the considered model parameters. Note that the  
 480 computing time is given as wall clock time for calculating the perturbations. Due to the parallelization of the computation, the total CPU time scales linearly with the number of cores used. Independent of the number of cores, the computational effort for calculating perturbations is low compared to running a model simulation. Despite small variations, the computing time increases linearly with the number of eigenmodes calculated. The required computational effort appears to increase approximately linearly with the number of sensitivities for covariance construction and the number of calculated eigenmodes. In this  
 485 case, doubling the number of considered sensitivities increases the computing time by about a factor of 2.3. Applying the

assumption of independent sensitivities reduces the number of used sensitivities in this study from 32 combined to 8 independent sensitivities including additional uncertainties. In addition to the strong reduction of computation time for simulating the sensitivities, the time for solving the eigenproblem reduces by about a factor of 4.5.

The results presented in this study demonstrate a considerable reduction of required computational resources under the assumption of independent sensitivities. As this method assumes linearity of parameter sensitivities, it may not be a sufficient approximation for all atmospheric parameters. However, the linear assumption relates to sensitivities of the perturbed parameters to model configurations. In other words, nonlinear effects resulting from the combination of different model arguments are disregarded. Note that this does not affect the impact of the parameters on prognostic fields like trace gas distributions and their propagation in time, which is beyond the ensemble generation and may still be highly nonlinear. Thus, the presented approach may also be suitable to be applied to parameters in NWP with highly nonlinear model dynamics. The sufficiency of this approximation for a model parameter in relation to the reduction of computational efforts needs to be evaluated for each specific application setup.

The developed KL approach may be extended to inverse optimization of model parameters. The generated parameter ensemble can be used to estimate state-dependent model covariances in an ensemble data assimilation system. If requested by the type of data assimilation algorithm, inverse square roots of covariance matrices are readily available for preconditioned minimization. Furthermore, the KL expansion of the parameter fields enables an advanced optimization approach. Instead of optimizing the parameter fields in its full  $N$ -dimensional space, the optimization can be performed in the reduced subspace spanned by the  $D$  leading eigenmodes. As the leading eigenmodes represent the dominant uncertainties of the parameters, the optimization would be restricted to those. In this case, the set of stochastic coefficients  $\{y_d\}_{d \in [1, D]}$  would be replaced by the optimization variable (compare Eq. (15)) which is fully determined by as low as  $D$  observations. Thus, this approach may be able to provide a rough, yet efficient optimization of model parameter fields with a low number of observations. For both optimization approaches, spurious correlations resulting from the restriction to leading uncertainties must be addressed by location measures.

## 6 Conclusions

This study introduces an optimized ensemble generation approach in which model parameters are efficiently perturbed according to their correlations. The approach is based on the fact that the forecast model acts as a dynamical system with its specific spatial and multivariate couplings of the atmospheric state. It applies the Karhunen-Loéve expansion which approximates covariances of the model parameters by a limited set of leading eigenmodes. These modes represent the coupled leading uncertainties from which perturbations can be sampled efficiently. Based on this, stochastic sampling for ensemble generation is performed in an uncorrelated subspace spanned by the eigenmodes. Generally, the presented algorithm is applicable to any set of model parameters in high-dimensional atmospheric systems, as long as their joint uncertainties remain in the linear regime. Through the reduction of the sampling space, it is shown that the stochastic dimension of the problem can be reduced significantly. This makes the algorithm suitable for efficient ensemble generation of high-dimensional atmospheric models, where the computational costs are a critical and limiting quantity.

Focusing on model parameters which depend on local environmental conditions, state-dependent covariances are approximated from various related sensitivities. Generally, the covariances required for this approach can be defined in any way which is suitable to reflect the uncertainty of our knowledge. Covariance construction based on parameter sensitivities as presented in this study is just one among others. Potential deficiencies in the construction could be identified from a posteriori evaluation of the full ensemble. This would allow for an ongoing adjustment of the algorithm depending on the specific application.

As simulations of all possible combinations of sensitivities are computationally demanding, independent sensitivities are introduced in this study. Assuming tangent-linearity, multiple combined sensitivities can be represented by a low number of independent sensitivities. Representative results indicate that the major properties of leading sensitivities are captured by independent sensitivities. **Considering 2 realizations of 6 model arguments, only 7 independent out of a total number of 64 combined sensitivities are required.** Thus, the method of independent sensitivities reduces the computational effort of model simulations prior to ensemble generation tremendously. Besides the reduction of computational resources, this method allows for the integration of different kinds of uncertainties in a convenient way. However in many cases, the assumption of independent sensitivities may not be a good approximation. The user has to decide if the computational benefit justifies the neglection of nonlinear effects.

The potential of the KL ensemble generation approach is investigated for regional forecasts of a set of biogenic emissions. During the selected case study in the Po valley in July 2012, biogenic emissions were exceptionally sensitive to several land surface properties. In this case, the eigenmode decomposition indicates high correlations of uncertainties in the regional domain as well as between different biogenic gases. Rapidly decreasing eigenvalues state the dominant contributions of only a few orthogonal components from a global point of view. Resulting perturbation factors for isoprene emissions created by the KL ensemble generation algorithm range between less than 0.1 up to 10. Although some realizations show common perturbation patterns, significant contributions from the subsequent eigenmodes can clearly be identified from the eight realizations. This indicates that the KL ensemble generation approach is able to sufficiently sample the subspace of leading uncertainties by only as low as 10 members in this case. Moreover, as each eigenmode represents common patterns of different sensitivities, the realizations are affected by the whole set of underlying sensitivities.

**A comprehensive evaluation of KL ensemble perturbations would be based on a representative amount of observational data. Comparing to observed trace gas concentrations requires the consideration of uncertainties related to different processes affecting those concentrations which is out of the scope of this study. Instead, the performance of the KL algorithm itself was evaluated using ensemble statistics. The statistical comparison of the KL perturbations with the sensitivities used as input states sufficient representation of the main aspects. Both, combined and independent methods, were able to capture the main uncertainties while smaller contributions were neglected according to the objective of the algorithm.**

The presented application of the KL ensemble generation approach demonstrates its potential for an efficient estimation of forecast uncertainties induced by model parameters in high-dimensional atmospheric models. Specifically, the presented algorithm allows for (1) an efficient estimation of various sensitivities based on the assumption of independent sensitivities, (2) an efficient extraction of leading coupled uncertainties using highly parallelized eigenmode decomposition, and (3) an efficient generation of perturbations of high-dimensional parameter fields by the Karhunen-Loéve expansion. This motivates

its promising application to various state-dependent parameters in chemistry transport modeling and potentially also in other  
555 atmospheric models. A follow up study will investigate and validate probabilistic forecasts of biogenic gases with respect to different state-dependent model parameters during the PEGASOS campaign in Po valley 2012. Furthermore, the approach may also be applied to other kinds of model parameters, where sufficient covariances need to be estimated accordingly. In this context, the reduction to leading coupled uncertainties offers the ability to account for dominant uncertainties across all parameters influencing atmospheric chemical forecasts. This would provide a significant step in the transition from deterministic to  
560 probabilistic chemistry transport modeling.

*Code and data availability.* The code of the KL ensemble generation algorithm available at <https://doi.org/10.5281/zenodo.4468571> (Vogel and Elbern, 2021b) contains the routines which are important for generating the results presented in this study. *The data used as input for the production of the results and the output of the algorithm are available at <https://doi.org/10.5281/zenodo.4772909> (Vogel and Elbern, 2021c).*

*Author contributions.* AV developed and implemented the algorithm, performed the simulations and wrote the manuscript. HE provided the  
565 basic idea, supervised the work, contributed to the developments and helped in the preparation of the manuscript.

*Competing interests.* The authors declare that they have no competing interests.

*Acknowledgements.* This work has been funded by the Helmholtz Climate Initiative REKLIM (Regional Climate Change), a joint research project of the Helmholtz Association of German research centers (HGF) under grant: REKLIM-2009-07-16. The authors gratefully acknowledge the computing time granted through JARA-HPC on the supercomputer JURECA (Jülich Supercomputing Centre, 2018) at  
570 Forschungszentrum Jülich. The authors thank the Institute of Geophysics and Meteorology at the University of Cologne for the opportunity to finish the work presented here. The authors thank two anonymous reviewers for their valuable suggestions.

## Appendix A: Derivation of Independent Mean and Covariance

Given a set of independent sensitivities  $\left\{x_i^s(r_i)\right\}_{\substack{r_i \in [1, R_i] \\ i \in [1, I]}}$  with implementation  $r_i \in [1, R_I]$  of each model argument  $i \in [1, I]$  at position  $s \in S$ . Assuming independence of sensitivities, each combined sensitivity  $X_j^s$  is given by

$$575 \quad X_j^s := X_{\{r_1, r_2, \dots, r_I\}}^s = \sum_{i=1}^I x_i^s(r_i) \quad \forall j \in [1, J], s \in S \quad , \quad (\text{A1})$$

where the total number of combined sensitivities is

$$J := \prod_{i=1}^I R_i \quad . \quad (\text{A2})$$

The **mean value**  $\mu(s)$  of all combined sensitivities  $\left\{X_j^s\right\}_{j \in [1, J]}$  at position  $s \in S$  can be calculated from the set of independent sensitivities  $\left\{x_i^s(r_i)\right\}_{\substack{r_i \in [1, R_i] \\ i \in [1, I]}}$  as follows:

$$\begin{aligned}
580 \quad \mu(s) &:= \frac{1}{J} \sum_{j=1}^J X_j^s \stackrel{(A2)}{=} \frac{1}{\prod_{i=1}^I R_i} \sum_{r_1=1}^{R_1} \sum_{r_2=1}^{R_2} \cdots \sum_{r_I=1}^{R_I} X_{\{r_1, r_2, \dots, r_I\}}^s \stackrel{(A1)}{=} \frac{1}{\prod_{i=1}^I R_i} \sum_{r_1=1}^{R_1} \sum_{r_2=1}^{R_2} \cdots \sum_{r_I=1}^{R_I} \left( \sum_{i=1}^I x_i^s(r_i) \right) \\
&= \frac{1}{J} \left( \left( x_1^s(1) + x_2^s(1) + \cdots + x_I^s(1) \right) + \left( x_1^s(1) + x_2^s(1) + \cdots + x_I^s(2) \right) + \cdots + \left( x_1^s(1) + x_2^s(1) + \cdots + x_I^s(R_I) \right) \right. \\
&\quad + \cdots \quad \vdots \quad \vdots \quad \vdots \quad \vdots \\
&\quad + \left( x_1^s(1) + x_2^s(2) + \cdots + x_I^s(1) \right) + \left( x_1^s(1) + x_2^s(2) + \cdots + x_I^s(2) \right) + \cdots + \left( x_1^s(1) + x_2^s(2) + \cdots + x_I^s(R_I) \right) \\
&\quad + \cdots \quad \vdots \quad \vdots \quad \vdots \quad \vdots \\
585 \quad &\quad + \left( x_1^s(1) + x_2^s(R_2) + \cdots + x_I^s(1) \right) + \left( x_1^s(1) + x_2^s(R_2) + \cdots + x_I^s(2) \right) + \cdots + \left( x_1^s(1) + x_2^s(R_2) + \cdots + x_I^s(R_I) \right) \\
&\quad + \left( x_1^s(2) + x_2^s(1) + \cdots + x_I^s(1) \right) + \left( x_1^s(2) + x_2^s(1) + \cdots + x_I^s(2) \right) + \cdots + \left( x_1^s(2) + x_2^s(1) + \cdots + x_I^s(R_I) \right) \\
&\quad + \cdots \quad \vdots \quad \vdots \quad \vdots \\
&\quad + \left( x_1^s(R_i) + x_2^s(1) + \cdots + x_I^s(1) \right) + \left( x_1^s(R_i) + x_2^s(1) + \cdots + x_I^s(2) \right) + \cdots + \left( x_1^s(R_1) + x_2^s(1) + \cdots + x_I^s(R_I) \right) \\
&\quad + \cdots \quad \vdots \quad \vdots \quad \vdots \\
590 \quad &\quad + \left( x_1^s(R_1) + x_2^s(R_2) + \cdots + x_I^s(R_I) \right) + \left( x_1^s(R_1) + x_2^s(R_2) + \cdots + x_I^s(R_I) \right) + \cdots + \left( x_1^s(R_1) + x_2^s(R_2) + \cdots + x_I^s(R_I) \right) \Bigg) \\
&= \frac{1}{\prod_{i=1}^I R_i} \left[ \left( \prod_{i=2}^I R_i \right) \cdot \left( \sum_{r_1=1}^{R_1} x_1^s(r_1) \right) + \left( \prod_{i=1| i \neq 2}^I R_i \right) \cdot \left( \sum_{r_2=1}^{R_2} x_2^s(r_2) \right) + \cdots + \left( \prod_{i=1}^{I-1} R_i \right) \cdot \left( \sum_{r_I=1}^{R_I} x_I^s(r_I) \right) \right] \\
&= \frac{1}{R_1} \cdot \left( \sum_{r_1=1}^{R_1} x_1^s(r_1) \right) + \frac{1}{R_2} \cdot \left( \sum_{r_2=1}^{R_2} x_2^s(r_2) \right) + \cdots + \frac{1}{R_I} \cdot \left( \sum_{r_I=1}^{R_I} x_I^s(r_I) \right) \\
&= \sum_{i=1}^I \left( \frac{1}{R_i} \cdot \sum_{r_i=1}^{R_i} x_i^s(r_i) \right) \tag{A3}
\end{aligned}$$

The covariance  $C(s, s')$  of all combined sensitivities  $\{X_j^s\}_{j \in [1, J]}$  at positions  $\tilde{s} = s, s' \in S$  can be calculated from the sets of independent sensitivities  $\{x_i^{\tilde{s}}(r_i)\}_{\substack{r_i \in [1, R_i] \\ i \in [1, I]}}$  as follows:

$$\begin{aligned}
C(s, s') &:= \frac{1}{J-1} \sum_{j=1}^J (X_j^s - \mu^s)(X_j^{s'} - \mu^{s'}) = \frac{1}{J-1} \left[ \sum_{j=1}^J (X_j^s \cdot X_j^{s'}) - \mu^s \left( \sum_{j=1}^J X_j^{s'} \right) - \mu^{s'} \left( \sum_{j=1}^J X_j^s \right) + J \cdot \mu^s \cdot \mu^{s'} \right] \\
&= \frac{1}{J-1} \left[ \sum_{j=1}^J (X_j^s \cdot X_j^{s'}) - \mu^s (J \cdot \mu^{s'}) - \cancel{\mu^{s'} (J \cdot \mu^s)} + \cancel{J \cdot \mu^s \cdot \mu^{s'}} \right] = \frac{1}{J-1} \left[ \sum_{j=1}^J (X_j^s \cdot X_j^{s'}) - J \cdot \mu^s \cdot \mu^{s'} \right] \\
&\stackrel{(A2)}{=} \frac{1}{J-1} \sum_{r_1=1}^{R_1} \sum_{r_2=1}^{R_2} \cdots \sum_{r_I=1}^{R_I} (X_{\{r_1, r_2, \dots, r_I\}}^s \cdot X_{\{r_1, r_2, \dots, r_I\}}^{s'}) - \frac{J}{J-1} \cdot \mu^s \cdot \mu^{s'} \\
&\stackrel{(A1)}{=} \frac{1}{J-1} \sum_{r_1=1}^{R_1} \sum_{r_2=1}^{R_2} \cdots \sum_{r_I=1}^{R_I} \left[ \left( \sum_{i=1}^I x_i^s(r_i) \right) \cdot \left( \sum_{i=1}^I x_i^{s'}(r_i) \right) \right] - \frac{J}{J-1} \cdot \mu^s \cdot \mu^{s'} \\
&\stackrel{(A3)}{=} \frac{1}{J-1} \sum_{i=1}^I \underbrace{\left( \prod_{l=1|l \neq i}^I R_l \right) \cdot \sum_{r_i=1}^{R_i} (x_i^s(r_i) \cdot x_i^{s'}(r_i))}_{\text{quadratic terms}} + \sum_{k=1|k \neq i}^I \underbrace{\left( \prod_{l=1|l \neq i, l \neq k}^I R_l \right) \cdot \sum_{r_i=1}^{R_i} \sum_{r_k=1}^{R_k} (x_i^s(r_i) \cdot x_k^{s'}(r_k))}_{\text{non-quadratic terms}} \\
&\quad - \frac{J}{J-1} \left[ \sum_{i=1}^I \left( \frac{1}{R_i} \cdot \sum_{r_i=1}^{R_i} x_i^s(r_i) \right) \right] \cdot \left[ \sum_{i=1}^I \left( \frac{1}{R_i} \cdot \sum_{r_i=1}^{R_i} x_i^{s'}(r_i) \right) \right] \\
&\stackrel{(A2)}{=} \frac{J}{J-1} \sum_{i=1}^I \left[ \frac{1}{R_i} \cdot \sum_{r_i=1}^{R_i} (x_i^s(r_i) \cdot x_i^{s'}(r_i)) + \sum_{k=1|k \neq i}^I \left[ \frac{1}{R_i \cdot R_k} \cdot \sum_{r_i=1}^{R_i} \sum_{r_k=1}^{R_k} (x_i^s(r_i) \cdot x_k^{s'}(r_k)) \right] \right] \\
&\quad - \frac{J}{J-1} \sum_{i=1}^I \left[ \frac{1}{(R_i)^2} \cdot \sum_{r_i=1}^{R_i} (x_i^s(r_i) \cdot x_i^{s'}(r_i)) + \sum_{k=1|k \neq i}^I \left[ \frac{1}{R_i \cdot R_k} \cdot \sum_{r_i=1}^{R_i} \sum_{r_k=1}^{R_k} (x_i^s(r_i) \cdot x_k^{s'}(r_k)) \right] \right] \\
&= \frac{J}{J-1} \sum_{i=1}^I \left[ \left( \frac{1}{R_i} - \frac{1}{(R_i)^2} \right) \cdot \sum_{r_i=1}^{R_i} (x_i^s(r_i) \cdot x_i^{s'}(r_i)) \right]
\end{aligned} \tag{A4}$$

605 **Appendix B: Setup of Combined Sensitivities**

**Table B1.** Overview of model setups used as combined sensitivities. A detailed description of the abbreviations and model implementations provided by Vogel and Elbern (2021a). The reference setup is denoted as \*, and deviations from this reference are written in bold letters ('PX' = Pleim-Xiu surface layer parameterization, 'Du' = Dudhia shortwave radiation parameterization).

land use	number	global	land surface	boundary layer	microphysics	radiation
USGS	1 *	ECMWF	Pleim-Xiu	MYJ+Eta	WSM6	RRTMG
USGS	2	ECMWF	RUC	MYJ+Eta	WSM6	RRTMG
USGS	3	ECMWF	Pleim-Xiu	ACM2+PX	WSM6	RRTMG
USGS	4	ECMWF	Pleim-Xiu	MYJ+Eta	TGS	RRTMG
USGS	5	ECMWF	Pleim-Xiu	MYJ+Eta	WSM6	Du+RRTM
USGS	6	ECMWF	RUC	ACM2+PX	WSM6	RRTMG
USGS	7	ECMWF	Pleim-Xiu	MYJ+Eta	TGS	Du+RRTM
USGS	8	ECMWF	RUC	ACM2+PX	TGS	Du+RRTM
USGS	9	GFS	Pleim-Xiu	MYJ+Eta	WSM6	RRTMG
USGS	10	GFS	RUC	MYJ+Eta	WSM6	RRTMG
USGS	11	GFS	Pleim-Xiu	ACM2+PX	WSM6	RRTMG
USGS	12	GFS	Pleim-Xiu	MYJ+Eta	TGS	RRTMG
USGS	13	GFS	Pleim-Xiu	MYJ+Eta	WSM6	Du+RRTM
USGS	14	GFS	RUC	ACM2+PX	WSM6	RRTMG
USGS	15	GFS	Pleim-Xiu	MYJ+Eta	TGS	Du+RRTM
USGS	16	GFS	RUC	ACM2+PX	TGS	Du+RRTM
MODIS	1	ECMWF	Pleim-Xiu	MYJ+Eta	WSM6	RRTMG
MODIS	2	ECMWF	RUC	MYJ+Eta	WSM6	RRTMG
MODIS	3	ECMWF	Pleim-Xiu	ACM2+PX	WSM6	RRTMG
MODIS	4	ECMWF	Pleim-Xiu	MYJ+Eta	TGS	RRTMG
MODIS	5	ECMWF	Pleim-Xiu	MYJ+Eta	WSM6	Du+RRTM
MODIS	6	ECMWF	RUC	ACM2+PX	WSM6	RRTMG
MODIS	7	ECMWF	Pleim-Xiu	MYJ+Eta	TGS	Du+RRTM
MODIS	8	ECMWF	RUC	ACM2+PX	TGS	Du+RRTM
MODIS	9	GFS	Pleim-Xiu	MYJ+Eta	WSM6	RRTMG
MODIS	10	GFS	RUC	MYJ+Eta	WSM6	RRTMG
MODIS	11	GFS	Pleim-Xiu	ACM2+PX	WSM6	RRTMG
MODIS	12	GFS	Pleim-Xiu	MYJ+Eta	TGS	RRTMG
MODIS	13	GFS	Pleim-Xiu	MYJ+Eta	WSM6	Du+RRTM
MODIS	14	GFS	RUC	ACM2+PX	WSM6	RRTMG
MODIS	15	GFS	Pleim-Xiu	MYJ+Eta	TGS	Du+RRTM
MODIS	16	GFS	RUC	ACM2+PX	TGS	Du+RRTM

## References

- Auger, L. and Tangborn, A.: A wavelet-based reduced rank Kalman filter for assimilation of stratospheric chemical tracer observations, *MONTHLY WEATHER REVIEW*, 132, 1220–1237, [https://doi.org/10.1175/1520-0493\(2004\)132<1220:AWRRKF>2.0.CO;2](https://doi.org/10.1175/1520-0493(2004)132<1220:AWRRKF>2.0.CO;2), 2004.

Bauer, P., Thorpe, A., and Brunet, G.: The quiet revolution of numerical weather prediction, *Nature*, 525, <https://doi.org/10.1038/nature14956>, 2015.

Bocquet, M., Elbern, H., Eskes, H., Hirtl, M., Carmichael, G., Flemming, J., Inness, A., Pagowski, M., Camañ, J., Saide, P., García, R., Sofiev, M., Vira, J., Baklanov, A., Carnevale, C., Grell, G., and Seigneur, C.: Data assimilation in atmospheric chemistry models:

Current status and future prospects for coupled chemistry meteorology models, *Atmospheric Chemistry and Physics*, 15, 5325–5358, <https://doi.org/10.5194/acp-15-5325-2015>, 2015.

- 615 Boynard, A., Beekmann, M., Foret, G., Ung, A., Szopa, S., Schmechtig, C., and Coman, A.: An ensemble assessment of regional ozone model uncertainty with an explicit error representation, *Atmospheric Environment*, 45, 784 – 793, <https://doi.org/https://doi.org/10.1016/j.atmosenv.2010.08.006>, <http://www.sciencedirect.com/science/article/pii/S135223101000659X>, 2011.
- 620 Buizza, R.: Introduction to the special issue on “25 years of ensemble forecasting”, *Quarterly Journal of the Royal Meteorological Society*, 145, 1–11, <https://doi.org/10.1002/qj.3370>, <https://rmets.onlinelibrary.wiley.com/doi/abs/10.1002/qj.3370>, 2019.
- Buizza, R., Tribbia, J., Molteni, F., and Palmer, T.: Computation of optimal unstable structures for a numerical weather prediction model, *Tellus A*, 45, 388–407, <https://doi.org/10.1034/j.1600-0870.1993.t01-4-00005.x>, <https://onlinelibrary.wiley.com/doi/abs/10.1034/j.1600-0870.1993.t01-4-00005.x>, 1993.
- 625 Buizza, R., Milleer, M., and Palmer, T. N.: Stochastic representation of model uncertainties in the ECMWF ensemble prediction system, *Quarterly Journal of the Royal Meteorological Society*, 125, 2887–2908, <https://doi.org/10.1002/qj.49712556006>, <https://rmets.onlinelibrary.wiley.com/doi/abs/10.1002/qj.49712556006>, 1999.
- Candiani, G., Carnevale, C., Finzi, G., Pisoni, E., and Volta, M.: A comparison of reanalysis techniques: Applying optimal interpolation and Ensemble Kalman Filtering to improve air quality monitoring at mesoscale, *Science of The Total Environment*, 458-460, 7 – 14, <https://doi.org/https://doi.org/10.1016/j.scitotenv.2013.03.089>, <http://www.sciencedirect.com/science/article/pii/S004896971300394X>, 2013.
- 630 Cohn, S. E. and Todling, R.: Approximate Data Assimilation Schemes for Stable and Unstable Dynamics, *J. Met. Soc. Japan*, 74, 63–75, 1996.
- Elbern, H., Strunk, A., Schmidt, H., and Talagrand, O.: Emission rate and chemical state estimation by 4-dimensional variational inversion, *Atmospheric Chemistry and Physics*, 7, 3749–3769, <https://doi.org/10.5194/acp-7-3749-2007>, <http://www.atmos-chem-phys.net/7/3749/2007/>, 2007.
- 635 Emili, E., Gürol, S., and Cariolle, D.: Accounting for model error in air quality forecasts: an application of 4DEnVar to the assimilation of atmospheric composition using QG-Chem 1.0, *Geoscientific Model Development*, 9, 3933–3959, <https://doi.org/10.5194/gmd-9-3933-2016>, 2016.
- Galin, M. B.: Study of the Low-Frequency Variability of the Atmospheric General Circulation with the Use of Time-Dependent Empirical 640 Orthogonal Functions, *Atmospheric and Oceanic Physics*, 43, 15–23, <https://doi.org/10.1134/S0001433807010021>, 2007.
- Gaubert, B., Coman, A., Foret, G., Meleux, F., Ung, A., Rouil, L., Ionescu, A., Candau, Y., and Beekmann, M.: Regional scale ozone data assimilation using an ensemble Kalman filter and the CHIMERE chemical transport model, *Geoscientific Model Development*, 7, 283–302, <https://doi.org/10.5194/gmd-7-283-2014>, <https://www.geosci-model-dev.net/7/283/2014/>, 2014.
- Geiger, H., Barnes, I., Bejan, I., Benter, T., and Spittler, M.: The tropospheric degradation of isoprene: An updated module for the regional 645 atmospheric chemistry mechanism, *Atmospheric Environment*, 37, 1503–1519, [https://doi.org/10.1016/S1352-2310\(02\)01047-6](https://doi.org/10.1016/S1352-2310(02)01047-6), 2003.
- Goris, N. and Elbern, H.: Singular vector-based targeted observations of chemical constituents: description and first application of the EURAD-IM-SVA v1.0, *GEOSCIENTIFIC MODEL DEVELOPMENT*, 8, 3929–3945, <https://doi.org/10.5194/gmd-8-3929-2015>, 2015.
- Guenther, A. B., Jiang, X., Heald, C. L., Sakulyanontvittaya, T., Duhl, T., Emmons, L. K., and Wang, X.: The Model of Emissions of Gases 650 and Aerosols from Nature version 2.1 (MEGAN2.1): an extended and updated framework for modeling biogenic emissions, *Geoscientific Model Development*, 5, 1471–1492, <https://doi.org/10.5194/gmd-5-1471-2012>, <https://www.geosci-model-dev.net/5/1471/2012/>, 2012.

- Guilloteau, C., Mamalakis, A., Vulis, L., Le, P. V. V., Georgiou, T. T., and Foufoula-Georgiou, E.: Rotated Spectral Principal Component Analysis (rsPCA) for Identifying Dynamical Modes of Variability in Climate Systems, *Journal of Climate*, 34, 715 – 736, <https://doi.org/10.1175/JCLI-D-20-0266.1>, <https://journals.ametsoc.org/view/journals/clim/34/2/JCLI-D-20-0266.1.xml>, 2021.
- Hanea, R., Velders, G., and Heemink, A.: Data assimilation of ground-level ozone in Europe with a Kalman filter and chemistry transport model, *JOURNAL OF GEOPHYSICAL RESEARCH-ATMOSPHERES*, 109, <https://doi.org/10.1029/2003JD004283>, 2004.
- Hanea, R. G. and Velders, G. J. M.: A hybrid Kalman filter algorithm for large-scale atmospheric chemistry data assimilation, *MONTHLY WEATHER REVIEW*, 135, 140–151, <https://doi.org/10.1175/MWR3269.1>, 2007.
- Hanna, S. R., Chang, J. C., and Fernau, M. E.: Monte carlo estimates of uncertainties in predictions by a photochemical grid model (UAM-IV) due to uncertainties in input variables, *Atmospheric Environment*, 32, 3619 – 3628, [https://doi.org/https://doi.org/10.1016/S1352-2310\(97\)00419-6](https://doi.org/https://doi.org/10.1016/S1352-2310(97)00419-6), <http://www.sciencedirect.com/science/article/pii/S1352231097004196>, 1998.
- Hannachi, A., Jolliffe, I. T., and Stephenson, D. B.: Empirical orthogonal functions and related techniques in atmospheric science: A review, *INTERNATIONAL JOURNAL OF CLIMATOLOGY*, 27, 1119–1152, <https://doi.org/10.1002/joc.1499>, 2007.
- Houtekamer, P. L., Lefavre, L., Derome, J., Ritchie, H., and Mitchell, H. L.: A System Simulation Approach to Ensemble Prediction, *Monthly Weather Review*, 124, 1225–1242, [https://doi.org/10.1175/1520-0493\(1996\)124<1225:ASSATE>2.0.CO;2](https://doi.org/10.1175/1520-0493(1996)124<1225:ASSATE>2.0.CO;2), [https://doi.org/10.1175/1520-0493\(1996\)124<1225:ASSATE>2.0.CO;2](https://doi.org/10.1175/1520-0493(1996)124<1225:ASSATE>2.0.CO;2), 1996.
- Jülich Supercomputing Centre: JURECA: Modular supercomputer at Jülich Supercomputing Centre, *Journal of large-scale research facilities*, 4, <https://doi.org/10.17815/jlsrf-4-121-1>, <http://dx.doi.org/10.17815/jlsrf-4-121-1>, 2018.
- Karhunen, K.: Über lineare methoden in der Wahrscheinlichkeitsrechnung, *Annales Academiae Scientiarum Fenniae*, 37, 3–79, 1947.
- Lehoucq, R. B., Sorensen, D. C., and Yang, C.: ARPACK Users Guide: Solution of Large Scale Eigenvalue Problems by Implicitly Restarted Arnoldi Methods., 1997.
- Leutbecher, M.: Ensemble size: How suboptimal is less than infinity?, *Quarterly Journal of the Royal Meteorological Society*, 145, 107–128, <https://doi.org/10.1002/qj.3387>, <https://rmets.onlinelibrary.wiley.com/doi/abs/10.1002/qj.3387>, 2019.
- Leutbecher, M., Lock, S.-J., Ollinaho, P., Lang, S. T. K., Balsamo, G., Bechtold, P., Bonavita, M., Christensen, H. M., Diamantakis, M., Dutra, E., English, S., Fisher, M., Forbes, R. M., Goddard, J., Haiden, T., Hogan, R. J., Juricke, S., Lawrence, H., MacLeod, D., Magnusson, L., Malardel, S., Massart, S., Sandu, I., Smolarkiewicz, P. K., Subramanian, A., Vitart, F., Wedi, N., and Weisheimer, A.: Stochastic representations of model uncertainties at ECMWF: state of the art and future vision, *Quarterly Journal of the Royal Meteorological Society*, 143, 2315–2339, <https://doi.org/10.1002/qj.3094>, <https://rmets.onlinelibrary.wiley.com/doi/abs/10.1002/qj.3094>, 2017.
- Liu, Y., Wang, L., Zhou, W., and Chen, W.: Three Eurasian teleconnection patterns: spatial structures, temporal variability, and associated winter climate anomalies, *CLIMATE DYNAMICS*, 42, 2817–2839, <https://doi.org/10.1007/s00382-014-2163-z>, 2014.
- Lock, S.-J., Lang, S. T. K., Leutbecher, M., Hogan, R. J., and Vitart, F.: Treatment of model uncertainty from radiation by the Stochastically Perturbed Parametrization Tendencies (SPPT) scheme and associated revisions in the ECMWF ensembles, *Quarterly Journal of the Royal Meteorological Society*, 145, 75–89, <https://doi.org/10.1002/qj.3570>, <https://rmets.onlinelibrary.wiley.com/doi/abs/10.1002/qj.3570>, 2019.
- Loéve, M.: Fonctions aleatoires du second ordre, *Processus Stochastiques et Mouvement Brownien*, 42e éd, 1948.
- McKeen, S., Chung, S. H., Wilczak, J., Grell, G., Djalalova, I., Peckham, S., Gong, W., Bouchet, V., Moffet, R., Tang, Y., Carmichael, G. R., Mathur, R., and Yu, S.: Evaluation of several PM2.5 forecast models using data collected during the ICARTT/NEAQS 2004 field study, *Journal of Geophysical Research: Atmospheres*, 112, <https://doi.org/10.1029/2006JD007608>, <https://agupubs.onlinelibrary.wiley.com/doi/abs/10.1029/2006JD007608>, 2007.

- Pöschl, U., Kuhlmann, R., Poisson, N., and Crutzen, P.: Development and Intercomparison of Condensed Isoprene Oxidation Mechanisms for Global Atmospheric Modeling, *Journal of Atmospheric Chemistry*, 37, 29–52, <https://doi.org/10.1023/A:1006391009798>, 2000.
- Schutgens, N. A. J., Miyoshi, T., Takemura, T., and Nakajima, T.: Applying an ensemble Kalman filter to the assimilation of AERONET observations in a global aerosol transport model, *Atmospheric Chemistry and Physics*, 10, 2561–2576, <https://doi.org/10.5194/acp-10-2561-2010>, <https://www.atmos-chem-phys.net/10/2561/2010/>, 2010.
- Schwab, C. and Todor, R. A.: Karhunen-Loève Approximation of Random Fields by Generalized Fast Multipole Methods, *J. Comput. Phys.*, 217, 100–122, <https://doi.org/10.1016/j.jcp.2006.01.048>, <https://doi.org/10.1016/j.jcp.2006.01.048>, 2006.
- 695 Shutts, G.: A kinetic energy backscatter algorithm for use in ensemble prediction systems, *Quarterly Journal of the Royal Meteorological Society*, 131, 3079–3102, <https://doi.org/10.1256/qj.04.106>, <https://rmets.onlinelibrary.wiley.com/doi/abs/10.1256/qj.04.106>, 2005.
- Siripatana, A., Mayo, T., Knio, O., Dawson, C., Le Maitre, O., and Hoteit, I.: Ensemble Kalman filter inference of spatially-varying Manning's n coefficients in the coastal ocean, *JOURNAL OF HYDROLOGY*, 562, 664–684, <https://doi.org/10.1016/j.jhydrol.2018.05.021>, 2018.
- 700 Skamarock, W. C., Klemp, J. B., Dudhia, J., Gill, D. O., Barker, D. M., Duda, M. G., Huang, X.-Y., Wang, W., and Powers, J. G.: A Description of the Advanced Research WRF Version 3, NCAR technical note, 2008.
- Sorensen, D.: Implicitly Restarted Arnoldi/Lanczos Methods for Large Scale Eigenvalue Calculations, in: *Parallel Numerical Algorithms. ICASE/LaRC Interdisciplinary Series in Science and Engineering*, edited by Keyes, D., Sameh, A., and V, V., vol. vol 4., Springer, Dordrecht, 1997.
- Toth, Z. and Kalnay, E.: Ensemble forecasting at NMC: The generation of perturbations, *Bulletin of the american meteorological society*, 74, 2317–2330, 1993.
- Vautard, R., Blond, N., Schmidt, H., Derognat, C., and Beekmann, M.: Multi-model ensemble ozone forecasts over Europe: analysis of uncertainty, *Mesoscale Transport of Air Pollution. OA15. EGS XXXVI General Assembly*. European Geophysical Society, Nice, France. Katlenburg-Lindau, Germany, 26, 2001.
- 710 Verlaan, M. and Heemink, A. M.: Data assimilation schmes for non-linear shallow water flow models, *Adv. Fluid Mech.*, 96, 277–286, 1996.
- Vogel, A. and Elbern, H.: Identifying forecast uncertainties for biogenic gases in the Po Valley related to model configuration in EURAD-IM during PEGASOS 2012, *Atmospheric Chemistry and Physics*, 21, 4039–4057, <https://doi.org/10.5194/acp-21-4039-2021>, <https://acp.copernicus.org/articles/21/4039/2021/>, 2021a.
- Vogel, A. and Elbern, H.: Karhunen-Loéve (KL) Ensemble Routines of the EURAD-IM modeling system, 715 <https://doi.org/10.5281/zenodo.4468571>, <https://doi.org/10.5281/zenodo.4468571>, 2021b.
- Vogel, A. and Elbern, H.: Data of Karhunen-Loéve (KL) ensemble generation algorithm for biogenic emissions from EURAD-IM, <https://doi.org/10.5281/zenodo.4772909>, <https://doi.org/10.5281/zenodo.4772909>, 2021c.
- Xian, P., Reid, J. S., Hyer, E. J., Sampson, C. R., Rubin, J. I., Ades, M., Asencio, N., Basart, S., Benedetti, A., Bhattacharjee, P. S., Brooks, M. E., Colarco, P. R., da Silva, A. M., Eck, T. F., Guth, J., Jorba, O., Kouznetsov, R., Kipling, Z., Sofiev, M., Perez Garcia-Pando, C., Pradhan, Y., Tanaka, T., Wang, J., Westphal, D. L., Yumimoto, K., and Zhang, J.: Current state of the global operational aerosol multi-model ensemble: An update from the International Cooperative for Aerosol Prediction (ICAP), *Quarterly Journal of the Royal Meteorological Society*, 145, 176–209, <https://doi.org/10.1002/qj.3497>, <https://rmets.onlinelibrary.wiley.com/doi/abs/10.1002/qj.3497>, 2019.
- Xiu, D.: *Numerical Methods for Stochastic Computations: A Spectral Method Approach*, Princeton University Press, Princeton, NJ, USA, 720 2010.

- 725 Zhang, Y., Bocquet, M., Mallet, V., Seigneur, C., and Baklanov, A.: Real-time air quality forecasting, part I: History, techniques, and  
current status, *Atmospheric Environment*, 60, 632 – 655, <https://doi.org/https://doi.org/10.1016/j.atmosenv.2012.06.031>, <http://www.sciencedirect.com/science/article/pii/S1352231012005900>, 2012a.
- Zhang, Y., Bocquet, M., Mallet, V., Seigneur, C., and Baklanov, A.: Real-time air quality forecasting, part II:  
State of the science, current research needs, and future prospects, *Atmospheric Environment*, 60, 656 – 676,  
730 <https://doi.org/https://doi.org/10.1016/j.atmosenv.2012.02.041>, <http://www.sciencedirect.com/science/article/pii/S1352231012001562>,  
2012b.